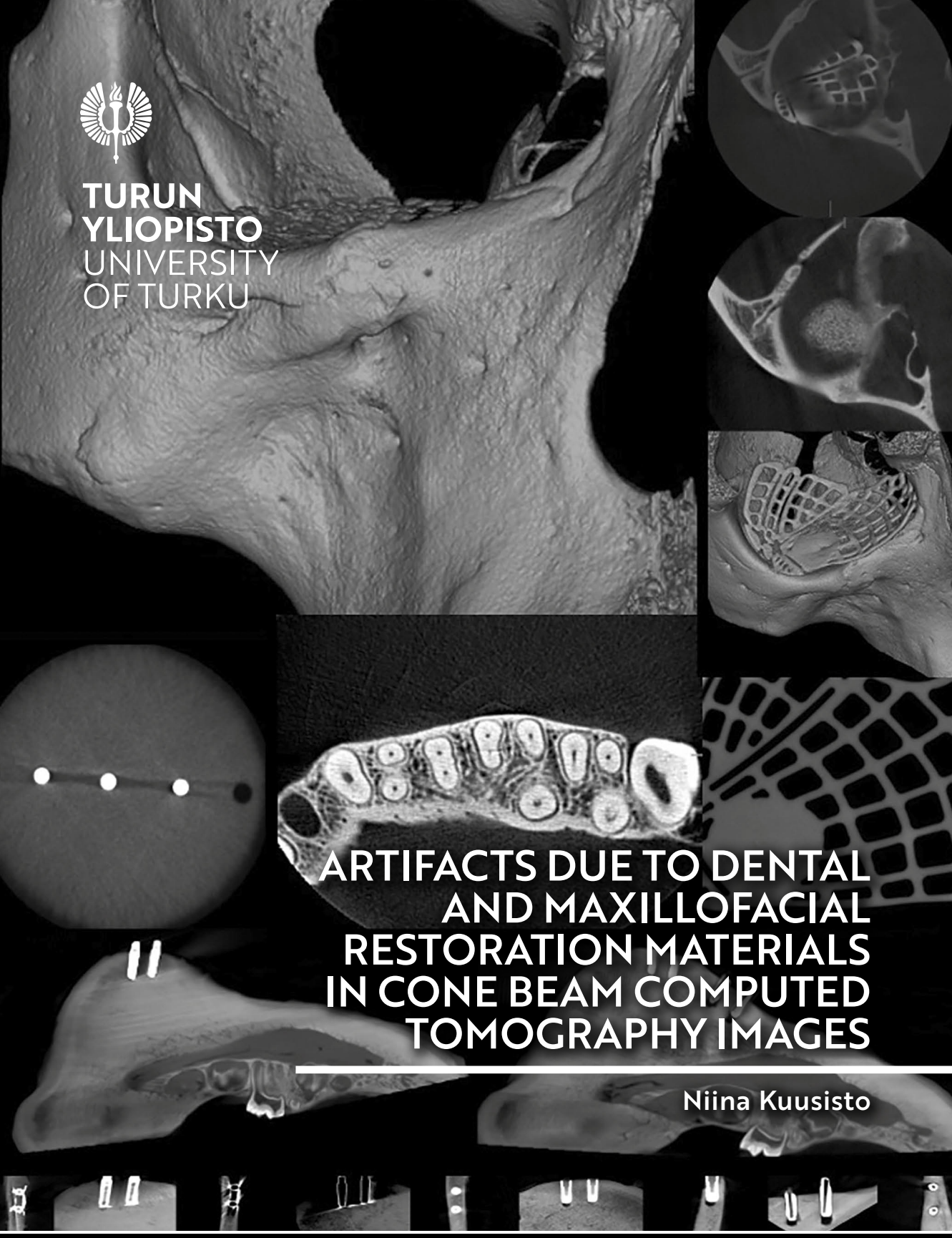

TURUN YLIOPISTO
UNIVERSITY OF TURKU

ARTIFACTS DUE TO DENTAL AND MAXILLOFACIAL RESTORATION MATERIALS IN CONE BEAM COMPUTED TOMOGRAPHY IMAGES

Niina Kuusisto

TURUN YLIOPISTON JULKAISUJA – ANNALES UNIVERSITATIS TURKUENSIS
SARJA – SER. D OSA – TOM. 1753 | MEDICA – ODONTOLOGICA | TURKU 2023

TURUN
YLIOPISTO
UNIVERSITY
OF TURKU

ARTIFACTS DUE TO DENTAL AND MAXILLOFACIAL RESTORATION MATERIALS IN CONE BEAM COMPUTED TOMOGRAPHY IMAGES

Niina Kuusisto

TURUN YLIOPISTON JULKAISUJA – ANNALES UNIVERSITATIS TURKUENSIS
SARJA – SER. D OSA – TOM. 1753 | MEDICA – ODONTOLOGICA | TURKU 2023

University of Turku

Faculty of Medicine, Institute of Dentistry
Department of Oral Pathology and Oral Radiology
Finnish Doctoral Programme in Oral Sciences (FINDOS-Turku)

Supervised by

Professor Sisko Huumonen
Institute of Dentistry
Faculty of Health Sciences
University of Eastern Finland
Kuopio, Finland

Professor Emerita Stina Syrjänen
Department of Oral Pathology and
Oral Radiology
Institute of Dentistry
Faculty of Medicine
University of Turku
Turku, Finland

Professor Pekka Vallittu
Department of Biomaterials Science
Institute of Dentistry
Faculty of Medicine
University of Turku and
Turku Clinical Biomaterials Centre (TCBC)
Turku, Finland

Reviewed by

Professor Reinhilde Jacobs
Department of Imaging and Pathology
OMFS-IMPATH Research Group
KU Leuven
Leuven, Belgium

Associate Professor Jaakko Sarin
Department of Medical Physics
Tampere University Hospital
The Wellbeing Services County of Pirkanmaa
Tampere, Finland

Opponent

Associate Professor Michaela Bode
Department of Radiology
Oulu University Hospital
The Wellbeing Services County of North Ostrobothnia
Oulu, Finland

The originality of this publication has been checked in accordance with the University of Turku quality assurance system using the Turnitin OriginalityCheck service.
Cover Image: Niina Kuusisto

ISSN 0355-9483 (Print)
ISSN 2343-3213 (Online)
ISBN 978-951-29-9500-4 (Print)
ISBN 978-951-29-9501-1 (PDF)
Painosalama, Turku, Finland 2023

UNIVERSITY OF TURKU
Faculty of Medicine
Institute of Dentistry
Department of Oral Pathology and Oral Radiology
NIINA KUUSISTO: Artifacts Due to Dental and Maxillofacial Restoration Materials in Cone Beam Computed Tomography Images
Doctoral Dissertation, 103 pp.
Finnish Doctoral Programme in Oral Sciences (FINDOS-Turku)
October 2023

ABSTRACT

Over the last 20 years, three-dimensional X-ray imaging, cone beam computed tomography (CBCT), has become an important method when making the diagnoses in the dental and maxillofacial area. There has been rapid development in CBCT devices, and the image quality has improved considerably during the last two decades. Despite the many improvements in CBCT image quality, artifacts induced by dental and maxillofacial restoration materials are still a problem, especially when diagnosing the dental area. CBCT manufacturers produce artifact reduction algorithms, which are intended to decrease or remove the artifacts in the image. However, the results of the studies on artifact reduction algorithms vary and there is no final consensus, as yet, on their efficacy. The studies of the present thesis focus on the artifacts induced by different dental and maxillofacial restoration materials in CBCT images. Another aim was to compare how the different materials interfere with the radiologic diagnosis. The materials investigated were titanium, zirconia, composite, and fiber reinforced composite (FRC).

The results showed that composites with radio-opacifying $BaAlSiO_2$ 20% (weight%) or more caused artifacts in the CBCT images. Composites with $BaAlSiO_2$ 68% (weight%) or more caused artifacts with similar intensity as titanium. Titanium orbital floor implant caused artifacts in the CBCT images, whereas nonmetallic fiber reinforced composite (FRC) orbital floor implant did not cause hampering artifacts in the CBCT images. The diagnosis of apical periodontitis can be complicated in 70% of the CBCT images of paranasal sinuses because of the artifacts induced by dental and endodontic restorations. In the CBCT images, zirconia dental implants caused intense artifacts despite the artifact reduction algorithm.

To conclude, different dental and maxillofacial restoration materials cause image hampering artifacts of different intensities in CBCT images. Zirconia is especially problematic in CBCT images. More studies are needed on artifact reduction methods to achieve an image quality without artifacts to make the correct diagnosis. In addition, the consequences of restoration and implant material options should be considered in postoperative CBCT images.

KEYWORDS: cone beam computed tomography, artifact, artifact reduction, titanium, zirconia, composite

TURUN YLIOPISTO
Lääketieteellinen tiedekunta
Hammaslääketieteen laitos
Suupatologia ja suuradiologia
NIINA KUUSISTO: Hampaiston ja kasvojen alueen restauraatiomateriaalien aiheuttamat artefaktat kartiokeilatietokonetomografiakuvissa
Väitöskirja, 103 s.
Kansallinen suun terveystieteiden tohtoriohjelma (FINDOS-Turku)
Lokakuu 2023

TIIVISTELMÄ

Kolmiulotteinen röntgenkuvausmenetelmä, kartiokeilatietokonetomografia (KKTT), on tullut tärkeäksi osaksi hampaiston ja kasvojen alueen diagnostiikkaa. KKTT-laitteet ovat kehittyneet ominaisuuksiltaan nopeasti ja kuvan laatu on parantunut viimeisen 20 vuoden aikana. Useista parannuksista huolimatta kuvan laatua haittaavat hampaiston ja kasvojen alueen restauraatiomateriaaleista aiheutuvat artefaktat etenkin hampaiston aluetta diagnosoitaessa. KKTT-laitteissa on valmistajien kehittämiä yksilöllisiä algoritmeja, joiden tarkoitus on vähentää tai poistaa artefaktoja. Näiden tutkimustulokset kuitenkin vaihtelevat eikä yhtenevää johtopäätöstä niiden toimivuudesta tai suositusta niiden käytöstä ole vielä olemassa. Tässä väitöskirjassa tutkittiin erilaisten hampaiston ja kasvojen alueen restauraatiomateriaalien aiheuttamia artefaktoja KKTT-kuvissa sekä artefaktojen aiheuttamia haittoja KKTT-kuvien diagnostiikassa. Tutkimuksissa käytetyt materiaalit ovat titaani, zirkonia, komposiitti ja kuitulujitteinen komposiitti (FRC).

Komposiitit, jotka sisälsivät radiopaakkista $BaAlSiO_2$ 20% (paino%) tai enemmän, aiheuttivat artefaktoja KKTT-kuvissa, ja komposiitit, jotka sisälsivät $BaAlSiO_2$ 68% (paino%) tai enemmän, aiheuttivat artefaktaa KKTT-kuvissa yhtä paljon kuin titaani. Titaanista oleva silmänpohjan implantti aiheutti artefaktaa KKTT-kuvissa, kun taas kuitulujitteisesta komposiitista oleva silmänpohjan implantti ei aiheuttanut merkittävää artefaktaa KKTT-kuvissa. Apikaaliparodontiitin diagnostiikka voi olla vaikeutunut 70% nenän sivuonteloiden KKTT-kuvissa hammastäytteiden ja endodonttisten täytteiden aiheuttamien artefaktojen vuoksi. KKTT-kuvissa zirkonia aiheuttaa erityisen voimakkaita artefaktoja, vaikka artefaktaa poistava algoritmi olisi käytössä.

Yhteenvetona voidaan todeta, että hampaiston ja kasvojen alueen restauraatiomateriaalit aiheuttavat voimakkuuksiltaan erilaisia artefaktoja KKTT-kuvissa. Etenkin zirkonia on ongelmallinen KKTT-kuvissa. Artefaktoja poistavia algoritmeja on syytä tutkia lisää, jotta saadaan diagnostisesti luotettava kuvanlaatu ilman artefaktoja. Hampaiston ja kasvojen alueen restauraatioiden ja implanttien materiaalivalintojen seuraukset postoperatiivisissa KKTT-kuvissa on hyvä huomioida.

AVAINSANAT: kartiokeilatietokonetomografia, artefakta, titaani, zirkonia, komposiitti

Table of Contents

Abbreviations **7**

List of Original Publications **9**

1 Introduction **10**

2 Review of the Literature **13**
2.1 Cone-beam Computed Tomography (CBCT) – Basics 13
2.1.1 Guidelines for Dental and Maxillofacial CBCT Imaging 13
2.2 CBCT Image Quality 14
2.2.1 Resolution and Noise 15
2.2.2 Imaging Parameters – Radiation Dose and Image Quality 15
2.2.3 CBCT Artifacts 16
2.2.4 Artifact Reduction Algorithms 17
2.3 Features of Dental Implant Materials 17
2.3.1 Titanium and Zirconia 18
2.3.2 Fiber Reinforced Composites (FRC) 19
2.3.3 FRC Implants 19
2.4 CBCT in Diagnosing Chronic Sinusitis, Apical Periodontitis and Peri-implantitis 20

3 Aims **23**

4 Materials and Methods **24**
4.1 Study Design 24
4.1.1 Phantoms and Implants (Study I, II, IV) 24
4.1.2 The Molds for Step Wedges and Implant Models (Study I) 29
4.1.3 Preparation of Composite Step Wedges and Implant Models (Study I, IV) 29
4.1.4 FRC Implant Model (Study IV) 30
4.1.5 Imaging Equipment and Imaging Parameters (Study I–IV) 31
4.2 Statistics (II–IV) 34

5 Results **35**
5.1 Intraoral Radiographs 35

5.2 CBCT Images 35
5.2.1 CBCT Findings in Study III 38
5.2.2 The Function of Artifact Reduction Algorithm ARA 40

6 Discussion 42
6.1 The Development of the CBCT Devices 42
6.1.1 CBCT Indications 42
6.1.2 CBCT Imaging Parameters and MAR Algorithms 43
6.1.3 Artifacts in the CBCT Images 44
6.2 Image Analysis 46
6.3 Limits and Prospects 46

7 Conclusions 48

Acknowledgements 49

References 51

Original Publications 59

Abbreviations

3D	Three-dimensional
2D	Two-dimensional
AI	Artificial intelligence
ALADAIP	"As low as diagnostically acceptable being indication-oriented and patient-specific"
ALARA	"As low as reasonably achievable"
ANOVA	Analysis of variance
AP	Apical periodontitis
ARA	Artifact reduction algorithm of Planmeca Viso G7
bis-GMA	Bisphenol-A diglycidyl methacrylate
bis-MEPP	Bisphenol-A ethoxylate dimethacrylate
BPO	Benzoyl peroxide
CBCT	Cone beam computed tomography
CRS	Chronic rhinosinusitis
CT	Computed tomography
DICOM	Digital imaging and communications in medicine
DRL	Diagnostic reference level
E-glass	Electrical glass
FBP	Filtered back projection
FDK	Feldkamp-Davis-Kress
FDP	Flat detector panel
FOV	Field of view
FRC	Fiber reinforced composite
HU	Hounsfield unit
ICC	Intraclass correlation coefficient
kPa	Kilopascal
kV	Kilovoltage
kVp	Kilovoltage peak
MAR	Metal artifact reduction
mA	Milliampere
MSCT	Multi-slice computed tomography

PACS	Picture archiving and communication systems
PMMA	Polymethyl methacrylate
RIS	Radiology information system
ROI	Region of interest
rpm	Rounds per minute
SEDENTEXCT	Safety and efficacy of a new and emerging dental X-ray modality
SD	Standard deviation
STUK	Säteilyturvakeskus, The Radiation and Nuclear Safety Authority
S-glass	Special high strength glass
TEGDMA	Triethyleneglycol dimethacrylate
TMJ	Temporomandibular joint
UDMA	Urethane dimethacrylate
w-%	Weight percentage

List of Original Publications

This dissertation is based on the following original publications, which are referred to in the text by their Roman numerals:

I Kuusisto N, Vallittu PK, Lassila LV, Huumonen S. Evaluation of intensity of artefacts in CBCT by radio-opacity of composite simulation models of implants in vitro. Dentomaxillofacial Radiology. 2015; 44: 20140157.

II Kuusisto N, Huumonen S, Kotiaho A, Haapea M, Rekola J, Vallittu P. Intensity of artefacts in cone beam CT examinations caused by titanium and glass fibre-reinforced composite implants. Dentomaxillofacial Radiology. 2019; 48: 20170471.

III Kuusisto N, Hirvonen J, Suominen A, Syrjänen S, Huumonen S, Vallittu P, Kinnunen I. Retrospective Analysis of Artifacts in Cone Beam Computed Tomography Images Used to Diagnose Chronic Rhinosinusitis. Diagnostics. 2023; 13: 1511.

IV Kuusisto N, Abushahba F, Syrjänen S, Huumonen S, Vallittu P, Närhi T. Zirconia implants interfere with the evaluation of peri-implant bone defects in cone beam computed tomography (CBCT) images even with artifact reduction. Dentomaxillofacial Radiology. 2023; 0: 20230252.

1 Introduction

Three-dimensional (3D) imaging is essential in the diagnosis of the complex anatomy of the dental and maxillofacial area. Two-dimensional (2D) dental and maxillofacial imaging - panoramic, skull and intraoral images, has limitations due to magnification, distortion, and superimposition of the anatomical structures, which sometimes can prevent the diagnostics (Scarfe & Farman, 2008). Cone-beam computed tomography (CBCT) enabled three-dimensional imaging in the dental and maxillofacial area in the late 1990s (Scarfe & Farman, 2008). The very first CBCT device for dental and maxillofacial imaging was the NewTom QR DVT 9000 (Quantitative Radiology, Verona, Italy) shown in Figure 1 (Angelopoulos et al., 2012). CBCT became popular in dentists' offices due to several advantages compared to computed tomography (CT), such as a lower radiation dose and a smaller physical size (Scarfe & Farman, 2008). In addition to the dental and maxillofacial area, CBCT imaging is also used to examine other small bone structures such as the middle ear, fingers, wrists, elbows, ankles, and knees (Casselman & Gieraerts, 2013). In addition to these, CBCT is applicated in many kinds of image guidance of surgical procedures (Scarfe & Farman, 2008).

During the last 20 years, CBCT has developed into a vital imaging method in the dental and maxillofacial area, and both the CBCT equipment and the software are developing rapidly (Angelopoulos et al., 2012; Scarfe & Farman, 2008). As an example of this, Figure 2 shows the latest version of the delicate CBCT equipment Viso G7 (Planmeca, Helsinki, Finland). According to Gaêta-Araujo and coworkers, there are 47 CBCT manufacturers located worldwide (Brazil, China, Denmark, Finland, France, Germany, Italy, Japan, Republic of Korea, Slovakia, Thailand, and USA) providing 279 CBCT models (Gaêta-Araujo et al., 2020). Despite the developments, there are, nevertheless, several types and sources of artifacts associated with CBCT that can decrease the image quality. Due to these artifacts, the image interpretation may be challenging and even misleading. The most common artifact, beam hardening, appears as streaks and dark shadings in CBCT images and is induced by dense materials used in dental restorations and orthodontic treatments such as crowns, brackets, and implants. For example, Mahesh and coworkers

investigated 365 CBCT images of which artifacts were found in 67.1% and beam hardening was the most prevalent artifact (Mahesh et al., 2022).

In oral, cranial, and maxillofacial implantology, titanium is the classic material of choice because of its good biocompatibility (Najeeb et al., 2019). Zirconia based implants have become widely used in dentistry because of their biocompatibility and esthetic color (Cionca et al., 2017). Composite based materials also have the required features for implant material and are thus under investigation as an new alternative implant material (Vallittu, 2018). Fiber reinforced composite (FRC) is a non-metallic composite which can provide a large number of possibilities in dentistry.

Metal artifact reduction (MAR) algorithms have been generated and are constantly being improved to manage the problem with CBCT artifacts. However, the results and the study setups of the algorithm research vary, and the ideal function of the algorithms in CBCT has yet to be developed. Alongside improved algorithms, innovative new implant materials may be the only solution to improve the image quality by decreasing the artifacts.

The focus of this thesis is to compare different dental and maxillofacial restoration materials in causing artifacts in CBCT images and the challenges involved in diagnosing these images. The main materials under investigations were titanium, zirconia, and fiber reinforced composite.

Figure 1. NewTom 9000 (Quantitative Radiology, Verona, Italy) was the first CBCT device for dental imaging. In this device the patient was positioned horizontally. With permission of Cefla Dental Group, Italy.

Figure 2. The latest CBCT Viso G7 (Planmeca, Helsinki, Finland) in which the patient is positioned standing. With permission of Planmeca, Helsinki.

2 Review of the Literature

2.1 Cone-beam Computed Tomography (CBCT) – Basics

The name CBCT originates from its cone-shaped X-ray beam. A CBCT unit has an X-ray tube and a detector attached in a so-called C-arm. This rotates once horizontally (180°-360°) around the patient, who is either seated or standing (Scarfe & Farman, 2008). The X-ray beam covers a cylindrical-shaped field of view (FOV) that is selected according to the region of interest. The sizes of the FOV vary depending on the CBCT device. The radiation is either continuous or pulsed and the benefit of the latter is an especially reduced radiation dose to the patient (Scarfe & Farman, 2008). Hundreds of 2D projection images are received during the examination. This is called raw data, and is required by the detector, which converts X-ray photons into an electrical signal. Different flat panel detectors (FPDs) are used in the current CBCT machines (Pauwels et al., 2015). The volumetric data is reconstructed with algorithms such as a filtered back projection. The Feldkamp-Davis-Kress (FDK) algorithm is the most used algorithm in CBCT devices (Feldkamp LA et al., 1984.; Scarfe & Farman, 2008). In addition, several variants of the simultaneous algebraic reconstruction technique (SART) are used (H. C. Lee et al., 2017). CBCT imaging typically takes 30 seconds or less. The complete CBCT image is viewed in three views, axial, sagittal and coronal (Scarfe & Farman, 2008). In addition, many kinds of 3D and 2D formats can be reconstructed.

2.1.1 Guidelines for Dental and Maxillofacial CBCT Imaging

Guidelines and indications for CBCT imaging have been issued by the Safety and efficacy of a new and emerging dental X-ray modality (SEDENTEXCT) Consortium 2012 (Radiation Protection 172, 2012). In addition, there are national guidelines in use, such as the National Guidance of Germany (R. Schulze, 2013), and The Radiation and Nuclear Safety Authority (STUK) provides instructions for CBCT application in Finland (J. Peltola et al., 2011). The SEDENTEXCT guidelines lists the 20 “basic principles”. According to the guidelines, CBCT can be considered if

the information in the 2D X-ray images is incomplete or does not correspond with the clinical findings. In addition, if only the bony structures are of interest, CBCT imaging is a recommendable alternative for multi-slice computed tomography (MSCT) because of the lower radiation dose. Developing dentition, restoring dentition, and surgical applications are the target categories of the SEDENTEXCT guidelines. These include the assessment of impacted teeth with or without a suspicion of associated resorption, cleft palates, surgery planning of orthodontic cases, endodontics, periodontal and periapical diseases, dental trauma, pre-surgical plan of implant insertion or removal of the third molars. In addition, defects in maxillary and mandibular bones and temporo-mandibular joint (TMJ) bony structures are included (Radiation Protection 172, 2012). According to the National German guidelines the pathologies of the paranasal sinuses should be detected with CBCT when this is not possible with 2D imaging.

There is an urgent need for up-dated guidelines for CBCT because of the technical development of the CBCT imaging and the expanded use of CBCT imaging during the past two decades as pointed out by Gaeta-Auraujo and coworkers in 2021 (Gaêta-Araujo et al., 2021). Also, according to Siiskonen and coworkers, the use of diagnostic reference levels (DRL) and the regular quality control of the CBCT devices should be paid attention (Siiskonen et al., 2021).

2.2 CBCT Image Quality

CBCT image quality is divided into subjective and objective factors. The subjective factor means a rating of the visibility of a specific anatomic structure. The objective factor means a measurement of a particular pattern in a phantom or test object (Scarfe & Angelopoulos, 2018). The main objective factors of image quality are spatial and contrast resolution, noise, and artifacts. In addition to a high-quality image, achieving the lowest radiation dose possible is essential. The principle of ALARA which stands for “as low as reasonably achievable” as well as the principle of ALADAIP “as low as diagnostically acceptable being indication-oriented and patient-specific” should be achieved (Goulston et al., 2016; Oenning et al., 2018; ‘The 2007 Recommendations of the ICRP, 2007).

In addition to image quality, cognitive overload, including time pressure, case complexity, clinical experience, knowledge and technical ability, can influence image interpretation errors and negatively impact diagnosis and treatment decisions (Hegde et al., 2023). However, more studies are needed on interpretative errors and the ways to prevent them.

2.2.1 Resolution and Noise

Resolution is divided into spatial resolution and contrast resolution. Spatial resolution means the capacity to distinguish structures near each other. Contrast resolution means the capacity to distinguish tissues or materials of different densities with different gray values (Scarfe & Angelopoulos, 2018). CBCT voxel size can range from 0.4 mm to 0.076 mm (Scarfe & Angelopoulos, 2018). CBCT images have isotropic voxels, the dimensions of which are equal in all directions. This enables accurate measurement in all dimensions (axial, coronal, and sagittal) without distortion or magnification (Scarfe & Farman, 2008) hence it is applicable for imaging small or thin osseous structures, such as teeth and facial bones (Scarfe & Farman, 2008). However, CBCT imaging is limited by its poor soft tissue contrast (Scarfe & Farman, 2008). The significant factor limiting the contrast resolution in CBCT is patient scatter radiation (Scarfe & Angelopoulos, 2018). The contrast resolution is measured in Hounsfield units (HU), and there are normalized HU values for air -1000 HU, and water 0 HU. However, in CBCT, HU values are unreliable and should be avoided in diagnosis (Pauwels, Araki, et al., 2015).

In CBCT image, noise represents the variation of the voxel values, which degrades the image quality (Pauwels, Araki, et al., 2015). Compared to CT, CBCT images are more susceptible to noise due to the wider beam geometry of CBCT (Pauwels, Araki, et al., 2015).

2.2.2 Imaging Parameters – Radiation Dose and Image Quality

The operating voltage of the X-ray generator of the CBCT varies from 40 to 120 kilovoltage peak (kVp) and the currents vary in the range of 1–32 milliamperes (mA) (Kiljunen et al., 2015). Current CBCT equipment have pre-fixed exposure protocols in which the tube current (mA), exposure time (s), FOV and kVp can be selected depending on the indication for imaging and patient size. Image quality and the radiation dose are dependent on the selected parameters. Spatial resolution can be improved by decreasing the voxel size. This causes more noise which can be reduced simultaneously by increasing the tube current (Pauwels, Araki, et al., 2015). However, the higher the tube current, the higher the radiation dose (Pauwels, Araki, et al., 2015). Noise is reduced by increasing the tube voltage, resulting in decreased contrast and a higher patient dose (Pauwels, Araki, et al., 2015). The large FOV of the CBCT image decreases the contrast and, at the same time, noise and artifacts are increased. The size of the FOV is recommend to equate with the region of interest (ROI) in order to achieve a lower radiation dose (Angelopoulos et al., 2012; Pauwels, Araki, et al., 2015; Rehani et al., 2015).

Moreover, different CBCT devices and protocols affect the image quality and the radiation doses. Radiation dose levels differ between and within the CBCT devices, and hence generalized dose comparisons between different devices or CBCT versus panoramic imaging etc. cannot be made (Gaêta-Araujo et al., 2020). A change in the settings in CBCT devices can even lead to a 50-fold dose difference (Jacobs, 2011; Oenning et al., 2018).

2.2.3 CBCT Artifacts

The definition of an artifact is a region seen in the image that does not equate with the object (Scarfe & Angelopoulos, 2018). In CBCT, several artifact types are present and their appearance varies between different CBCT equipment (Codari et al., 2017). Artifacts can appear as streaks, shadings, rings, or bands (Hsieh, 2003). These can deteriorate the image quality by obscuring the anatomy, mimicking pathology, affecting the measurements, and misleading the diagnosis.

Multiple artifacts are caused when the X-ray interact with high density materials. These include dental restoration materials, metal alloys and composites, and implant materials including titanium and zirconia.

Scatter is seen as streaks after the image reconstuction, and it is produced by diffracted X-ray photons after interaction with the object (R. Schulze et al., 2011). This is corrected by various algorithms in CBCTs (Pauwels, Araki, et al., 2015).

Beam hardening is a common artifact in CBCT images seen as streaks and dark shadings around and between the high-density materials (De Man et al., 1999). This is caused by the increased effective kV as it passes the high density-object when only X-rays with low energy are absorbed. Beam hardening can be divided into two forms, a cupping artifact and streaks and dark bands. Cupping originates from cylindrical objects – X-rays which pass through the center of the cylindrical object lead stronger beam hardening than those that pass through the margins of the object. Dark shadings around and between high-density materials are caused by beam hardening, X-rays that go through only one object or several high-density objects. Bright lines, streak artifacts also originate from high-density materials and these can extend to wide area in the image. (Scarfe & Angelopoulos, 2018)

Extinction artifacts or missing value artifacts appear as dark areas when a high-density object absorbs the whole X-ray beam (R. Schulze et al., 2011). The exponential edge gradient effect is characterized by thin lines originating from high-density materials with sharp edges (Scarfe & Angelopoulos, 2018). Scanner-related artifacts are seen as rings in the axial plane caused by imperfections in the scanner detector or calibration errors (Scarfe & Angelopoulos, 2018). A partial volume effect, under sampling (aliasing) and a cone-beam effect are caused by the geometry

of the beam projection and the image reconstruction. This is characterized as streaks and shadings in the image (Scarfe & Angelopoulos, 2018), (Scarfe & Farman, 2008).

A motion artifact is one of the main causes that decreases the image quality, and it occurs when the patient moves during the CBCT examination. Because of the relatively long examination time, motion artifacts are quite frequent. In the image, this appears as unsharp or with double contours (Scarfe & Farman, 2008). The motion also strengthens metal artifacts (Nardi et al., 2015). Various algorithms and methods for reducing motion artifacts have been studied to be effective (Eldib et al., 2018; Sun et al., 2021).

A metal artifact is a term used for artifacts resulting from metallic, high-density materials. Metal artifacts originate from multiple effects - beam hardening and exponential edge-gradient effect as well as scatter, noise, and photon starvation (De Man et al., 1999; R. Schulze et al., 2011). Metal artifact reduction (MAR) algorithms have been developed and are constantly being improved to manage this problem.

2.2.4 Artifact Reduction Algorithms

Artifact reduction, or metal artifact reduction (MAR) algorithms have been generated to improve image quality using mathematical models and advanced reconstruction techniques (Bal & Spies, 2006; Kalender et al., 1987; Meyer et al., 2010). Generally, MAR algorithms are divided into different methods of which projection modification method is favored at the moment (Liugang et al., 2020; Zhang et al., 2007). Projection modification method detects the metal artifacts in the raw data and replaces them with estimated values (Zhang et al., 2007). The corrected image is obtained by reconstructing the corrected sinogram using the filtered back projection (FBP) (Liugang et al., 2020).

The performance of the algorithms has been extensively studied, but the results and the study setups vary, so a unanimous recommendation for their use cannot be made. However, most recent studies recommend the MAR algorithm (de Faria Vasconcelos et al., 2020; Fontenele et al., 2020). A comparative evaluation is still required to achieve an ideal performance of the algorithms and understand their limitations.

2.3 Features of Dental Implant Materials

Implants in the maxillofacial area fix fractures and defects and maintain the volume and function. Dental implants replace missing teeth and maintain occlusion and performance. The material of the dental implant has multiple requirements to maintain its functional stability. In addition to the biocompatibility, multiple stress types are affecting the material, such as tensile, compression, shear, and torsional

stress (P. Vallittu & Özcan, 2017). The modulus of elasticity should be comparable to the bone to ensure the distribution of the stress at implant and to prevent implant movement (Amarnath et al., 2011; Saini, 2015). High yield strength and fatigue strength as well as toughness prevent brittle fractures and wear under cyclic loading (Saini, 2015; P. Vallittu & Özcan, 2017).

In addition, materials have different radiological behavior. There are different ways in which X-rays interact with matter. The photons, bundles of energy, can scatter completely with no energy loss, be absorbed with a total loss of energy, scatter with some absorption and loss of energy or transmit unchanged (Whaites & Drage, 2015). Dense materials with a high atomic number are strong absorbers and are seen as very bright in the image, i.e. radiopaque. Materials of low atomic number absorb weakly allowing the photons to go through. These materials are seen as dark in the image, i.e. radiolucent (Mallya et al., 2019). The X-ray image expresses the X-ray attenuation of the different materials depending on the differences in material density (atomic number), thickness, as well as quality (kV) of the radiation beam (Whaites & Drage, 2015). The effective atomic number for soft tissue is approximately seven and for bone is approximately 12 (Whaites & Drage, 2015). Lead is used in the radiation protection because of the high atomic number (82) (Whaites & Drage, 2015).

2.3.1 Titanium and Zirconia

Titanium and titanium alloys have long been successful as implant materials. As a dental implant material, commercially pure titanium is the most common (Najeeb et al., 2019). Titanium is biocompatible, especially due to a stable oxide layer on its surface, and it fulfils the requirements of an implant material (Sykaras et al., 2000; Tschernitschek et al., 2005). The well-known disadvantage of titanium is its gray color which may cause esthetic problems when soft tissue is thin (Tschernitschek et al., 2005). Another widely studied disadvantage of titanium is the artifacts in the CBCT images (Benic et al., 2013; Pauwels et al., 2013; R. K. W. Schulze et al., 2010).

Compared to titanium implants, zirconium dioxide implants have shown to pose several advantages (Comisso et al., 2021). The color of zirconia is more esthetic compared to titanium, and it is assumed to have a lower risk for peri-implant diseases (Cionca et al., 2017; Özkurt & Kazazoğlu, 2011). However, zirconia implants are shown to create even more detrimental artifacts in the CBCT images than titanium (Demirturk Kocasarac et al., 2022; R. Schulze, 2022). This can be explained by the atomic number of zirconium (40) and titanium (22) (R. Schulze, 2022) which means, that a zirconia implant absorbs more X-ray energy leading to greater artifacts.

Summarized by Rajendran and coworkers, materials with high atomic number cause more beam hardening (Rajendran et al., 2014).

2.3.2 Fiber Reinforced Composites (FRC)

Fiber reinforced composites (FRC) have been an area of interest for a few decades in dentistry. FRCs meet all the mechanical, chemical, and esthetical requirements of the oral environment (Akalın-Evren et al., 2014; Bijelic-Donova et al., 2015; Cacciafesta et al., 2007; Foek et al., 2013; Kumbuloglu et al., 2008; P. K. Vallittu, 2018). Compared to metallic implant materials FRCs have properties closer to the bone tissue (Wang et al., 2021). FRC is composed of a polymeric matrix (polymethyl methacrylate or bisphenol A-glycidyl methacrylate (Bis-GMA) and triethylene glycol dimethacrylate (TEGDMA) and reinforcing fibers (Varley et al., 2019). The fibers are commonly referred to as Electrical glass, i.e. E-glass, or Special high strength glass, i.e. S-glass. The fibers can be oriented in variable ways - continuous unidirectional, plane-oriented bidirectional weave, or plane random fibers (P. Vallittu & Özcan, 2017). According to Garoushi and coworkers, short fibers that are randomly orientated function as reinforcement in all directions (S. K. Garoushi, Lassila, & Vallittu, 2006). Furthermore, by increasing the number of fibers the mechanical properties can be improved (Abdulmajeed et al., 2011). FRCs are widely applicable in dentistry used in removable prosthodontics (Ladizesky et al., 1994), fixed prosthodontics (Loose et al., 1998; P. K. Vallittu, 1998), periodontology (Agrawal & Chitko, 2011; S. Garoushi et al., 2008; Sewón et al., 2000), endodontics (Lassila et al., 2004; Le Bell-Rönnlöf et al., 2011), orthodontics (Rantala et al., 2003; P. K. Vallittu, 2016), restorative dentistry (Butterworth et al., 2003; S. K. Garoushi, Lassila, Tezvergil, et al., 2006), and in repairs of fixed prostheses (Özcan et al., 2006; P. Vallittu & Özcan, 2017). In addition, FRCs can be customized pre-operatively before the polymerization which enables an individual and precise fit (M. J. Peltola et al., 2012; Tuusa et al., 2008).

2.3.3 FRC Implants

The application of FRCs has also been investigated as an implant material and bone substitute, such as cranioplasty implants (Piitulainen et al., 2017), orbital floor implants and craniofacial bone reconstruction (Lazar et al., 2016). In addition, FRCs are being investigated in orthopedics, trauma and spine surgery and dental implantology (Vallittu, 2018).

Orbital floor and cranial FRC implants comprise of composite, layers of glass fiber network and bioactive glass granules in the center of the implant. The structure is mesh-like, with space between the outer and inner laminates filled with bioactive

glass particles (P. K. Vallittu, 2017). The network-like structure enables ossification and vascularization (P. K. Vallittu, 2017). The success of the cranial FRC implants has been verified by experimental studies (Aitasalo et al., 2014; Piitulainen et al., 2015; Posti et al., 2016; Tuusa et al., 2008).

All restorative composite materials should be visible in all X-ray images. The minimum required radio-opacity of restorative materials is determined by the international standard (ISO International standard 4049, 2009).

2.4 CBCT in Diagnosing Chronic Sinusitis, Apical Periodontitis and Peri-implantitis

CRS with a Dental Origin

Chronic rhinosinusitis (CRS) and chronic rhinosinusitis with a dental origin are difficult to differentiate because of their similar symptoms, such as pain, nasal discharge and postnasal drip and nasal obstruction (Matsumoto et al., 2015). In addition, CRS with a dental origin is a diagnosis without a clear criterion, thus making the exact diagnosis challenging. It is estimated that chronic rhinosinusitis has a dental origin in 70% of unilateral paranasal sinusitis cases (Matsumoto et al., 2015). CRS and CRS with a dental origin have different bacterial microbiomes (Puglisi et al., 2011; Saibene et al., 2016). This is why, the origin and etiology of CRS is of importance when selecting the appropriate treatment, such as dental surgery, medical treatment or endoscopic sinus surgery (Little et al., 2018; Saibene et al., 2016).

Damage in the maxillary sinus mucoperiosteum caused by apical periodontitis (AP), periodontal disease, oroantral fistula, misplaced roots or foreign bodies in the sinus are the causes of CRS from a dental origin (Vidal et al., 2017; Zirk et al., 2017). Among these, AP is the usual cause, presumably due to the anatomy - maxillary molar roots and maxillary sinus floor being located nearby each other (Vidal et al., 2017; Zirk et al., 2017). In addition to AP, 2 mm or more thick unilateral mucosal thickening on the maxillary sinus floor is a radiological sign to suggest CRS with a dental origin (Shanbhag et al., 2013; Vidal et al., 2017). CBCT or CT imaging is essential for diagnosing the dental origin of CRS.

Apical Periodontitis

Apical periodontitis (AP) originates from an infected pulp located in the periapical area of the root (Meirinhos et al., 2020). This disorder usually occurs due to dental caries or trauma (Sasaki et al., 2016). Molars are often associated with AP, especially those with root fillings (Meirinhos et al., 2020). AP symptoms and clinical signs vary

from no symptoms to destruction of the underlying bone with or without an abscess. According to Tibúrcio-Machado and coworkers, approximately half of the adults worldwide have had AP at least in one tooth (Tibúrcio-Machado et al., 2021). Patients with systemic diseases, such as diabetes, or previous endodontic treatments, have a higher incidence of AP (Nagendrababu et al., 2020; Tibúrcio-Machado et al., 2021).

AP is diagnosed from the dental radiographs appearing first as a widened or highlighted periodontal ligament in the apical area of the root. As the infection progresses, the periapical tissues, periodontal ligament and alveolar bone, are destroyed, causing periodontal lesions (Nair, 2004). Because the host defensive system cannot reach into the complex root canal system, AP is not a self-healing disorder and needs special treatments, such as endodontic therapy or removal of the tooth (Nair, 1997). If not treated, AP can lead to CRS or so-called odontogenic sinusitis. The maxillary first molars are more often associated with the maxillary sinus floor changes than the other maxillary teeth (Maillet et al., 2011).

Peri-implantitis

Osseointegration, a special bond between the bone and the implant, is required for dental implants to maintain their functional stability (Reti & Findlay, 2021). Osseointegration is dependent on the bone quality, the surface of the implant, as well as the health of the patient, and the implant loading and position (Reti & Findlay, 2021). The implant success includes the absence of mobility, symptoms, and infection. In the X-ray images, the vertical bone loss should not reach more than 0.2 mm after the first year, and peri-implant radiolucency should not be present (Reti & Findlay, 2021).

Bone loss and inflammation of the soft tissue around a dental implant are the characteristics of peri-implantitis. Clinically, bleeding or suppuration on probing, and a probing depth more than 5 mm are present in peri-implantitis. In addition, erythema, hyperplasia, swelling and the mobility of the implant may be present (Reti & Findlay, 2021). Based on the studies, the prevalence of peri-implantitis is currently more than 20% (Derks & Tomasi, 2015; C.-T. Lee et al., 2017). In the oral environment, dental implants are continuously exposed to microbes. Peri-implantitis is prevented only by a frequent plaque control of the implant (Salvi & Ramseier, 2015).

Gradually peri-implantitis can cause vertical bone loss and radiolucency around the implant. At first, horizontal and one wall mesiodistal vertical bone defects can be seen in intraoral radiographs. However, buccal and lingual/palatal vertical bone loss cannot be seen in two-dimensional X-ray images (Rees et al., 1971). CBCT imaging can be considered in more complicated cases, such as fenestration,

dehiscence, or three wall bone defects (Bayat et al., 2016; Christiaens et al., 2018; Jacobs et al., 2018). In CBCT images, the artifacts caused by implants are seen as radiolucency around and between the implants. Vertical bone loss around the implant may not be recognized in CBCT images since the metal artifacts exist exactly in the same area. Due to artifacts, CBCT is not recommended as a primary imaging method when peri-implantitis is suspected, and intraoral radiography is still recommended for monitoring dental implants (Jacobs et al., 2018).

3 Aims

Objectives of the Study

The aim of the present studies was to investigate the artifact formation caused by different implant materials and how these artifacts challenge the diagnostics of the CBCT images. Furthermore, the usefulness of the metal artifact reduction method in CBCT imaging was tested.
The specific objectives were:

I To compare the artifacts induced by titanium, zirconia and seven models of composite dental implants containing varying amounts of radiopacifying $BaAlSiO_2$ in CBCT images.

II To compare the artifacts in CBCT images induced by the orbital floor implants of titanium and FRC.

III To retrospectively examine the frequency of artifacts and their influence on the diagnosis of chronic rhinosinusitis and apical periodontitis in the CBCT images of paranasal sinuses.

IV To examine the function of the metal artifact reduction method (ARA) of the Planmeca Viso G7 CBCT device with pairs of titanium, zirconia and FRC dental implants.

4 Materials and Methods

Artifacts induced by different dental restoration materials in CBTC images were investigated in three experimental studies (Studies I, II and IV) and in one clinical retrospective study (III). The materials and methods used in these four different studies are summarized in Table 1 and 2.

4.1 Study Design

4.1.1 Phantoms and Implants (Study I, II, IV)

In Study I, a Teflon block was used to hold titanium, zirconia, and composite dental implant models (Figure 3.). In Study II, titanium and FRC orbital floor implants were set on to the orbital floor of a dry human skull as shown in Figure 4. The shape and the size of the implants were not exactly equal; details given in Table 1. A piece of cardboard was used to support the skull at the optimal position during the CBCT scanning.

Figure 3. Teflon block and the titanium implant models used in Study I.

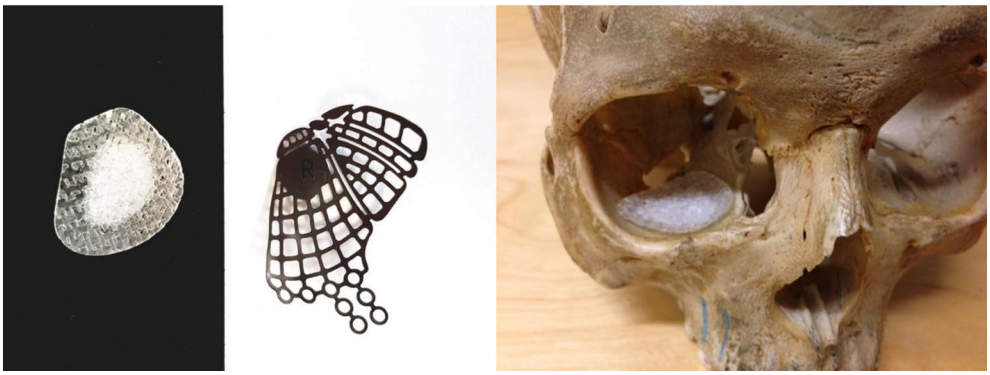

Figure 4. Left: The FRC and titanium orbital floor implants. Right: The skull used in Study II to support the orbital floor implants. From the original publication II with permission of DMFR.

In Study IV, two titanium (Straumann® Bone Level Implant, Straumann Holding AG, Basel Switzerland), zirconia (Straumann® PURE Ceramic Implant Monotype, Straumann Holding, AG, Basel Switzerland) and handmade FRC (University of Turku, Turku, Finland) dental implants (size 3.3 × 10 mm) were placed at a 5 mm distance from each other in a pig mandible lacking soft tissues. The implants were installed according to the manufacturer's instructions (Straumann Holding AG). The titanium and FRC implants were set into the opposite side of the mandible to the zirconia implants. The defect that simulated peri-implantitis, was made by drilling on the buccal side of one implant of each material (3 mm in width, 5 mm in height, 1 mm in depth). The other (control) implant of each material was installed without any defect, as shown in Figure 5.

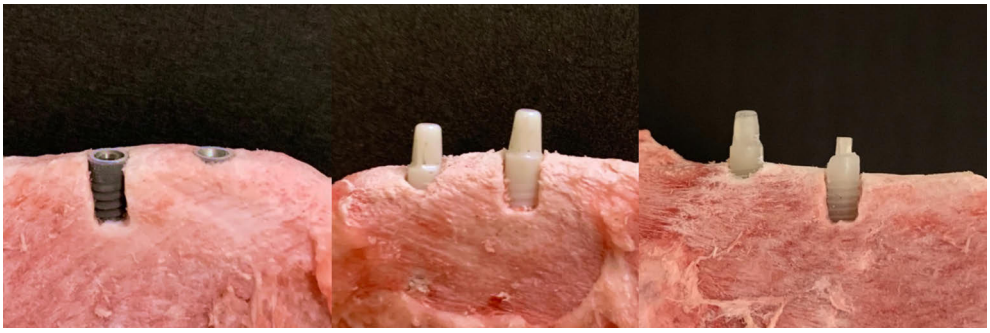

Figure 5. From left: Dental implants of titanium, zirconia and FRC. The design of the defects is seen in one of each of the implants.

Table 1. Materials and methods in the Studies I-IV.

Study	Study design	Imaging equipment	Imaging parameters	MAR	Software for image analysis	Image observation	Statistics
I	Experimental study Teflon block Aluminium, titanium, zirconia and composite step wedges (TCBC, Turku, Finland) Titanium, zirconia and composite cylinders 20 mm in height and 3 mm in thickness (TCBC, Turku, Finland)	Planmeca Intra X-ray (Planmeca, Helsinki, Finland) CBCT, SCANORA 3D (Soredex, Tuusula, Finland)	63 kV, 5–8 mA, 0.08–0.2 s 90 kV, 12 mA, 7.43 s, FOV 5 × 5 cm, 150 μm	-	ImageJ (National Institutes of Health, Bethesda, MD)	Bachelor of Dental Sciences Axial view of the CBCT image	-
II	Experimental study Dry human skull (Institute of Dentistry, University of Turku, Finland), Orbital floor implants: Titanium MatrixORBITAL 35 × 40 × 0.4 mm (DePuy Synthe, Oberdorf, Switzerland) FRC size L 24 × 29 × 0.5–1.5 mm (Glace, Skulle Implants Corporation, Turku, Finland)	CBCT, 3D Accuitomo 170, (Morita, Kyoto, Japan)	80 kV, 1 mA, 7 s, FOV 6 × 6 cm, 125 μm The sizes of the ROIs pixels (base x height) ROI1 2697 (3.8 × 13.8 mm) ROI2 2880 (14.4 × 3.9 mm) ROI3 1224 (13.5 × 1.4 mm)	-	ImageJ (National Institutes of Health, Bethesda, MD) Matlab (R2016b, The MathWorks, Natick, MA)	1) Bachelor of Dental Sciences 2) Oral and Maxillofacial Radiologist ROI 1–3, the axial views of the CBCT images	ANOVA, Tukey's test, Games-Howell's test, Benjamini-Hochberg method, SPSS 23 (IBM, NY, USA)
III	Clinical retrospective study 214 CBCT images of paranasal sinuses (DM1AI) taken during 2017 at the Emergency Radiology unit in the Turku University Hospital Age ≥ 50 years, CRS as the indication	CBCT, Planmed Verity (Planmed, Helsinki, Finland)	96 kV, 6 mA, 8 s, FOV 16 × 13 cm, 200 μm	-	RIS, PACS	1) Oral and Maxillofacial Radiologist 2) Head and Neck Radiologist Both observers made the visual analysis once. Axial, sagittal, and coronal views of the CBCT image were analyzed.	ICC, SPSS 29 (IBM, NY, USA)

IV	Experimental study Frozen pig mandible without soft tissues Titanium 3.3 × 10 mm (Straumann Bone Level Implant, Straumann Holding AG, Basel Switzerland) Zirconia 3.3 × 10 mm (Straumann PURE Ceramic Implant Monotype, Straumann Holding AG, Basel Switzerland) FRC handmade, see Table 2.	CBCT, Planmeca Viso G7 (Planmeca, Helsinki, Finland)	100 kV, 12 mA, 5 s, FOV 22 × 12 cm, 300 μm 90 kV, 14 mA, 4.5 s, FOV 5 × 5 cm, 150 μm 100 kV, 12 mA, 12.8 s, FOV 5 × 5 cm, 75 μm	ARA (0–3)	Romexis Viewer 6 (Planmeca, Helsinki, Finland)	1) Oral and Maxillofacial Radiologist 2) Bachelor of Dental Sciences Both observers made the measurements once. Axial, sagittal, and coronal views of the CBCT image were analyzed.	ICC, SPSS 29 (IBM, NY, USA)

CBCT, cone-beam computed tomography; FOV, field of view; FRC, fiber reinforced composite; ROI, region of interest; ANOVA, analysis of variance; CRS, chronic rhinosinusitis; RIS, radiology information system; PACS, picture archiving and communication systems; ICC, intra class correlation coefficient; ARA, artifact reduction algorithm of Planmeca Viso G7

Table 2. The materials used for the composite models and the implant compositions.

Study	Materials for preparing the composite models	Manufacturer	Implant composition
I	Mold of step wedges: Putty Soft polyvinyl siloxane, impression material Affinis Precious Aluminium step wedge (TCBC, Turku, Finland) Mold of dental implants: Lab Putty and Lab Putty Catalyst Titanium cylinder 20 mm in height and 3 mm in thickness (TCBC, Turku, Finland)	Coltene/Whaledent, Alstätten, Switzerland	Seven step wedges and composite dental implant models: $BaAlSiO_2$ weight% + SiO_2 weight% + composite resin (Bis-GMA 70% + TEGDMA 30% + 1% BPO) 1. 68% + 0% 2. 64% + 6% 3. 57% + 14% 4. 47% + 25% 5. 32% + 38% 6. 20% + 49% 7. 0% + 74%
II	Titanium and FRC orbital floor implants	Titanium MatrixORBITAL 35×40×0.4 mm, pure Titanium (DePuy Synthe, Oberdorf, Switzerland) FRC size L 24×29×0.5-1.5 mm (Glace, Skulle Implants Corporation, Turku, Finland)	FRC: perforated S-glass, (nominal composition in wt%: SiO_2 62–65; Al_2O_3 20–25; MgO 10–15; B_2O_3 0–1.2; Na_2O 0–1.1; FeO_3 0.2) Dimethacrylate polymer matrix and bioactive glass particles (S53P4; nominal composition in wt%: Na_2O 24.5; CaO 24.5; SiO_2 45; P_2O_5 6) The average particle size of the bioactive glass 400 µm Glass fiber loading in the dimetacrylate matrix 60 vol%
IV	Translucent polyvinyl siloxane Zirconia 3.3 x 10 mm (Straumann PURE Ceramic Implant Monotype) FRC	Exaclear, GC, Tokyo, Japan Straumann Holding AG, Basel Switzerland everStick C&B, Stick Tech-GC Group, Turku, Finland everX Flow, bulk shade, GC, Tokyo, Japan	Zirconia: 100% yttria-stabilized zirconia (Y-TZP) FRC: continuous E-glass (SiO_2 54wt%, Al_2O_3 14wt%, CaO+MgO 22wt%, B_2O_3 10wt% and Na_2O+K_2O less than 2wt%) + bis-GMA + PMMA (everStick C&B) discontinuous short E-glass + bis-MEPP, TEGDMA and UDMA (everX Flow)

Bis-GMA, bisphenol-A diglycidyl methacrylate; TEGDMA, triethyleneglycol dimethacrylate; BPO, benzoyl peroxide; FRC, fiber reinforced composite; PMMA, polymethyl methacrylate; UDMA, urethane dimethacrylate; bis-MEPP, bisphenole-A ethoxylate dimethacrylate; E-glass, electrical glass

4.1.2 The Molds for Step Wedges and Implant Models (Study I)

Materials used for preparing the molds are shown in Table 2. The mold for composite step wedges (Study I) was prepared by mixing one manufacturer's scoop of Putty Soft Base and Putty Soft Catalyst (Coltene/Whaledent, Altstätten, Switzerland). The putty mixture was placed in a glass bowl (Fig. 6.). An aluminium step wedge was covered with impression material (Affinis® Precious, Coltene/Whaledent) and then pressed into the putty mixture; it was then left to harden for 3 minutes. The mold for dental implant models was made in the same way as the mold for step wedges by mixing one manufacturer's measuring scoop each of Lab Putty and the Lab Putty Catalyst (Coltene/Whaledent). A pure titanium rod (20 mm in length, 3 mm in diameter) was pressed into the Putty mixture and the mold was let harden for 5 min. Impression material was not needed for this mold.

4.1.3 Preparation of Composite Step Wedges and Implant Models (Study I, IV)

The composition of the composite step wedges and dental implant models (Study I) are shown in detail in Table 2. The composite step wedges and dental implant models contained seven varying amounts of SiO_2 and $BaAlSiO_2$ (Table 2.). SiO_2 and $BaAlSiO_2$ were mixed with the resin, blended in a speed mixer at 1700 rpm for 30 s (SpeedMixer, DAC 150 FVZ; Hauschild, Germany), and repeated until the composite was able to be manipulated. The composite was set into the molds and pressed with sheet glass and polymerized for 15min in a pressure curing unit at 100 °C in 200 kPa (Ivomat IP12, Ivoclar ag.; Schaan, Liechtenstein). Composite implant models were finished to equate with the dimensions of the titanium rod (Fig. 7.).

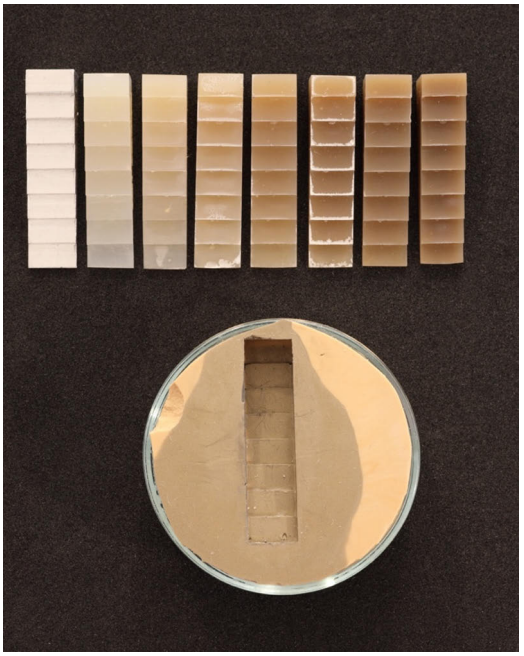

Figure 6. Aluminium step wedge was used to prepare the seven (1–7) composite step wedges and the mold. The steps were 1–8 mm thick.

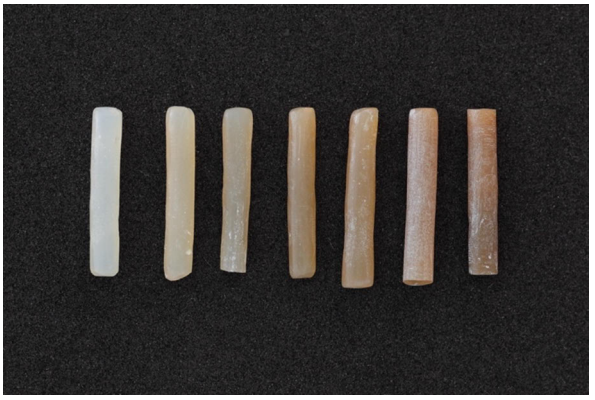

Figure 7. Seven composite dental implant models. The implant Model 1 on the far left contains the highest concentration $BaAlSiO_2$ while the implant Model 7 on the far right, contains no $BaAlSO_2$.

4.1.4 FRC Implant Model (Study IV)

A Straumann's zirconia implant was used as a model for preparing two glass fiber reinforced composite replicas in Study IV. The split mold, made of translucent polyvinyl siloxane (Exaclear, GC, Tokyo, Japan), was filled with dimethacrylate

resin, continuous unidirectional E-glass fiber rovings (everStick C&B, Stick Tech-GC Group, Turku, Finland) and discontinuous E-glass fiber reinforced composite (everX Flow, bulk shade, GC, Tokyo, Japan) (Table 2.). Polymerization of the implant was made with a LED light-curing unit (Elipar S10, 3M ESPE, St. Paula, MN, USA) with light intensity of 1765 mW/cm^2. The light curing tip was in contact with the transparent polyvinyl siloxane mold during the polymerization time of 40 seconds.

4.1.5 Imaging Equipment and Imaging Parameters (Study I–IV)

The step wedges of the Study I were imaged with Planmeca Intra X-ray (Planmeca, Helsinki, Finland) next to an aluminium step wedge with the imaging parameters shown in Table 1. The dental implant models were set in three groups into the Teflon block and imaged with CBCT SCANORA 3D (Soredex, Tuusula, Finland) with the imaging parameters shown in Table 1. ImageJ (National Institutes of Health, Bethesda, MD) acquired the average gray values of the composite step wedges in intraoral radiographs with a pixel point analysis to compare each step with the aluminium steps illustrated in Figure 8. CBCT axial slices (1 mm) were also analyzed with ImageJ. The variation in the gray values was demonstrated as a cross-sectional line through the implants shown in Figure 9.

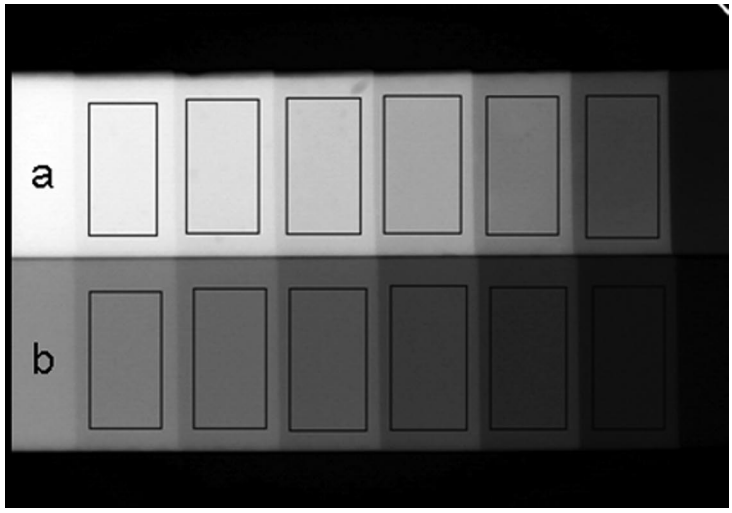

Figure 8. Intraoral image of the composite step wedge (**a**) and aluminium step wedge (**b**). From the original publication I, with permission of DMFR.

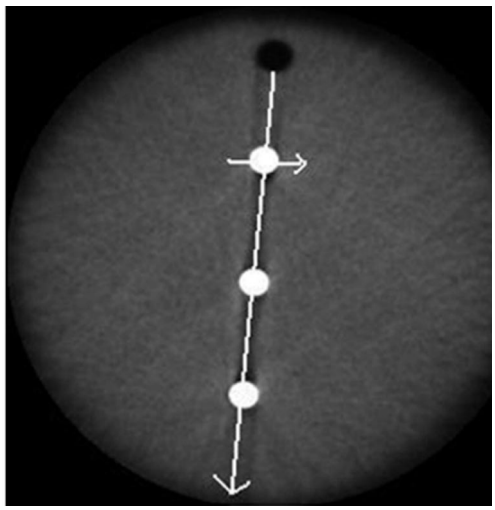

Figure 9. Titanium implant models set into the Teflon block. The arrows show the cross-sectional line from the original publication I, with permission of DMFR.

In Study II, the orbital floor implants supported by a skull were examined with CBCT 3D Accuitomo 170 (Morita, Kyoto, Japan). The imaging parameters used are presented in Table 1. The CBCT images were transferred to Matlab (Matlab R2016b, The MathWorks, Natick, MA) in the form of digital imaging and communications in medicine (DICOM) to create the ROIs. The anatomic structures of the skull with and without the implants were in the same position in the images. Based on the artifacts seen in the CBCT image with the titanium implant, three parallelogram shaped regions of interest (ROI) were created (Fig. 10). The magnitude of the artifacts was examined in nine subsequent transversal slices. ROI 1 was created on the anterior side of the implant, ROI 2 on the lateral and ROI 3 on the medial side of the implant.

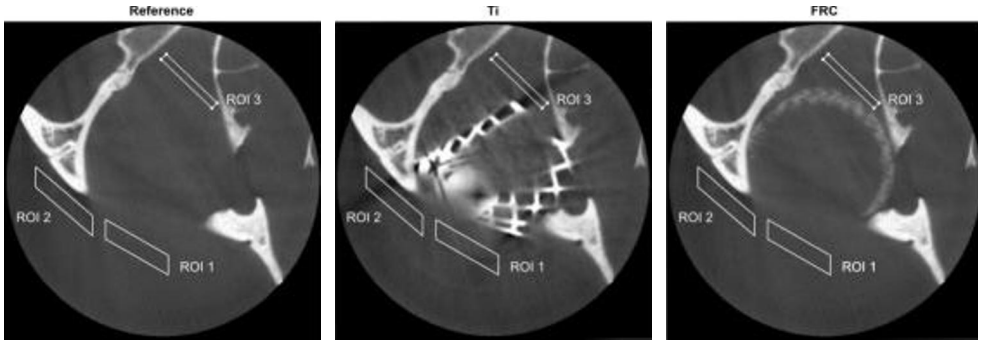

Figure 10. From left to right: ROIs 1–3 around the orbital floor, titanium and FRC implants. From the original publication II with permission of DMFR.

In the retrospective study (Study III), 214 CBCT images of paranasal sinuses (code DM1AI) taken in 2017 were collected from the Emergency Radiology unit at Turku University Hospital. Patients under 50 years of age were excluded from the sample. The CBCT device and the parameters used are shown in Table 1. Two radiologists with different subspecialties – oral and maxillofacial radiology and head and neck radiology performed the image analysis. The medical reports and referrals confirmed the diagnosis of CRS and AP. In the CBCT images, the artifacts were registered (yes/no) if they hampered identifying the anatomy or the diagnosis of CRS and AP in only one slice of the cross-sectional view. The artifacts were investigated in all three orthogonal views and in three areas delimited by anatomical landmarks shown in Figure 11. Regarding the anatomy, the identification of the periodontal ligament spaces of the premolar and molar roots (level 1), the cortex of the maxillary sinus walls (level 2) and the cortex of the paranasal sinuses (level 3) were required. Regarding the diagnosis of CRS, the identification of a mucosal thickening of 2 mm or more was required. Regarding the diagnosis of AP, the identification of a highlighted periodontal ligament or a radiolucent change in the periapical area was required. The restoration materials, such as, implants, crowns and endodontic fillings and posts were identified visually, but different restoration materials could not be differentiated from each other in the CBCT images. A dental filling was graded large when it extended to at least three sides of the crown.

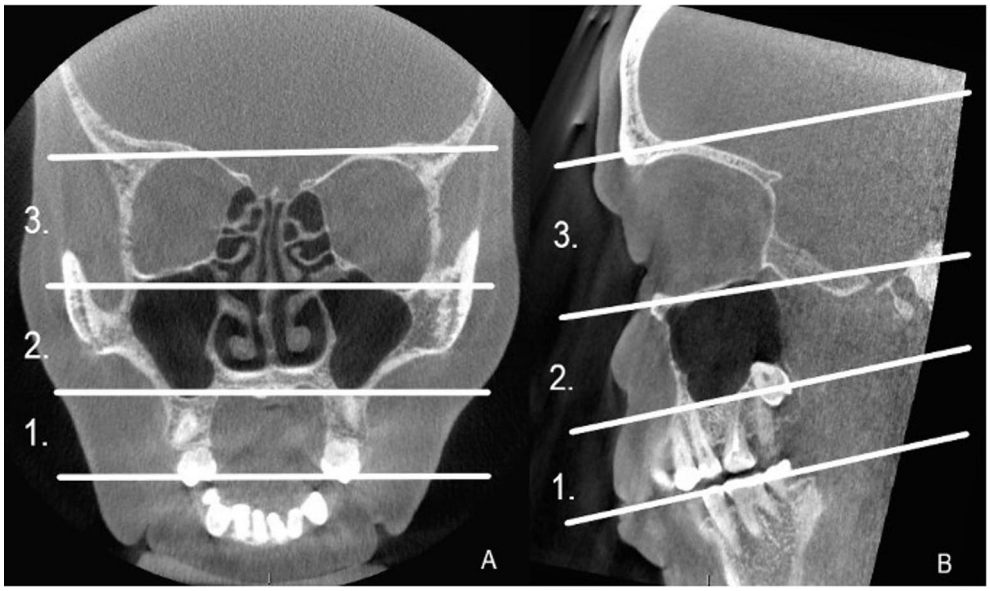

Figure 11. The CBCT image slices demonstrating levels 1–3 **A**) coronal and **B**) sagittal view. Level 1 covers the area from the premolar-molar crowns to the maxillary sinus floor. Level 2 covers the maxillary sinus to the orbital floor and level 3 covers the orbit to the orbital roof. From the original publication III with permission of Diagnostics.

In Study IV the implants inserted into the pig mandible were imaged with CBCT Planmeca Viso G7 (Planmeca, Helsinki, Finland) using three imaging parameters as given in Table 1. Three different levels of the metal artifact reduction (ARA) were used with all the imaging parameters. An oral and maxillofacial radiologist (Observer 1) and a Bachelor of Dental Sciences, BDS (Observer 2) under the same calibrated conditions analyzed the images. The defect was analyzed in all three orthogonal views – the height and caudal depth were measured in the coronal view, and the width in the axial view of the CBCT image. The defect was measured with the measuring tool in Romexis Viewer (Romexis Viewer 6, Planmeca, Helsinki, Finland). The bone structure and the marginal cortex had to be seen as smooth and intact between the implant pairs (yes/no). About the implant structure, the spiral part was analyzed visually (yes/no). Observers analyzed the CBCT images using an Eizo RadiForce GX340 diagnostic monitor with 3 megapixels and a resolution of 1536 × 2048 (Eizo Nanao Corporation, Ishikawa, Japan).

4.2 Statistics (II–IV)

Statistical analyses were performed in the Studies II–IV with the tests given in Table 1. SPSS v.23 was used in the Study I and SPSS 29 was used in the Studies III and IV (IBM, Armonk, NY, USA).

Briefly, in Study II, the mean gray values between the CBCT images with and without the implants in ROIs 1–3 were compared using a one-way analysis of variance (ANOVA). The differences in the CBCT image without the implant and with the FRC or titanium implant were calculated using a Tukey's test (equal variances between the groups) or Games-Howell's test (un-equal variances between the groups). The Benjamini-Hochberg method corrected multiple comparisons separately for ROIs. P-values less than 0.05 were considered statistically significant. In Study III and IV, interobserver agreement was calculated by the ICC test (interobserver class correlation coefficient). In Study III, 50 CBCT images were randomly selected.

5 Results

5.1 Intraoral Radiographs

The gray value comparisons of the step wedges in the intraoral images were proceeded to clarify their differences in X-ray images. The average gray value differences of the aluminium, zirconia, and composite step wedges (1–3 mm) are presented in Figure 12. Gray values of the composite step wedges 1 and 2 are close to each other and the composite step wedges 3 and 4. The composite step wedge 7 had the lowest gray values, while zirconia had the highest gray values.

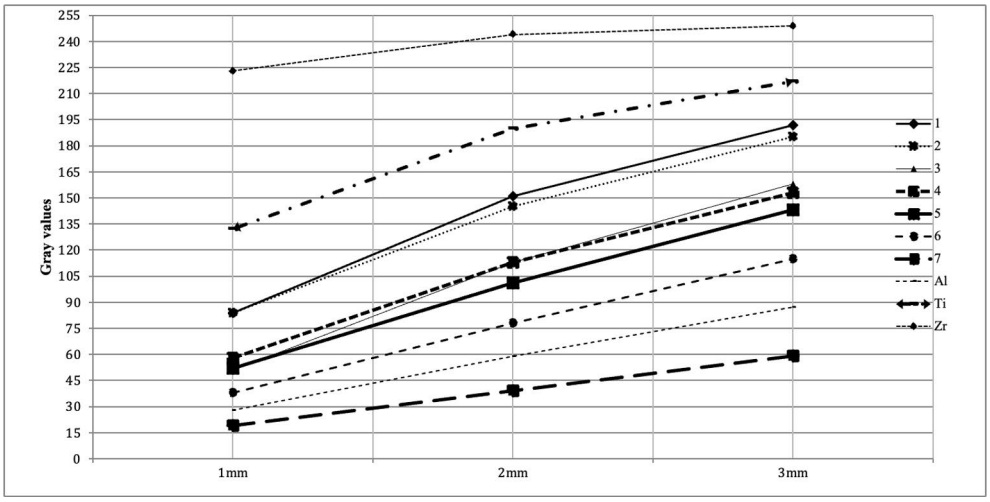

Figure 12. The average gray values of the step wedges in the intraoral images. From the original publication I, with permission of DMFR.

5.2 CBCT Images

Composites containing $BaAlSiO_2$ less than 20% and FRC orbital floor implant did not cause any image hampering artifacts in the CBCT images (Study I–II). Table 3 summarizes the origins of the artifacts in Studies I–IV and their disadvantages in the CBCT images.

Table 3. The origins of the artifacts and their disadvantages in the CBCT images as found in Studies I–IV.

Study	The origin of the artifacts	The disadvantage in the CBCT image
I	Zirconia and titanium implant models Composites with $BaAlSiO_2$ 20% or more Composites with $BaAlSiO_2$ 68% or more	Bright streaks and dark bands around and between the implant models
II	Titanium orbital floor implant	Dark bands around the implant
III	Dental restorations, endodontic fillings, dental implants, other maxillofacial implants	Bright streaks, dark areas, and inaccuracy Recognizing the teeth anatomy and the diagnosis of apical periodontitis was complicated
IV	Zirconia implants	Large dark areas and bright streaks around the implants The bone around the implants was not identified

The artifacts induced by dental implant models in Study I were compared in the axial CBCT slices and gray value cross-sections shown in Figure 13. Zirconia implant models caused the most intense artifacts in the CBCT images seen as bright streaks and dark bands around and between the implants. Titanium implant models induced pronounced artifacts in the CBCT images seen also as bright streaks and dark bands between the implant models. Of the composite implant models 1 and 2 caused the most pronounced artifacts in the CBCT images followed by the models 3 and 4. Composite implant models caused mainly dark bands between the implants. Implant models 5 and 6 caused only minor artifacts in CBCT images. The composite model 7 did not contain any $BaAlSiO_2$, thus its gray values were the lowest and it did not cause any artifacts in the CBCT images.

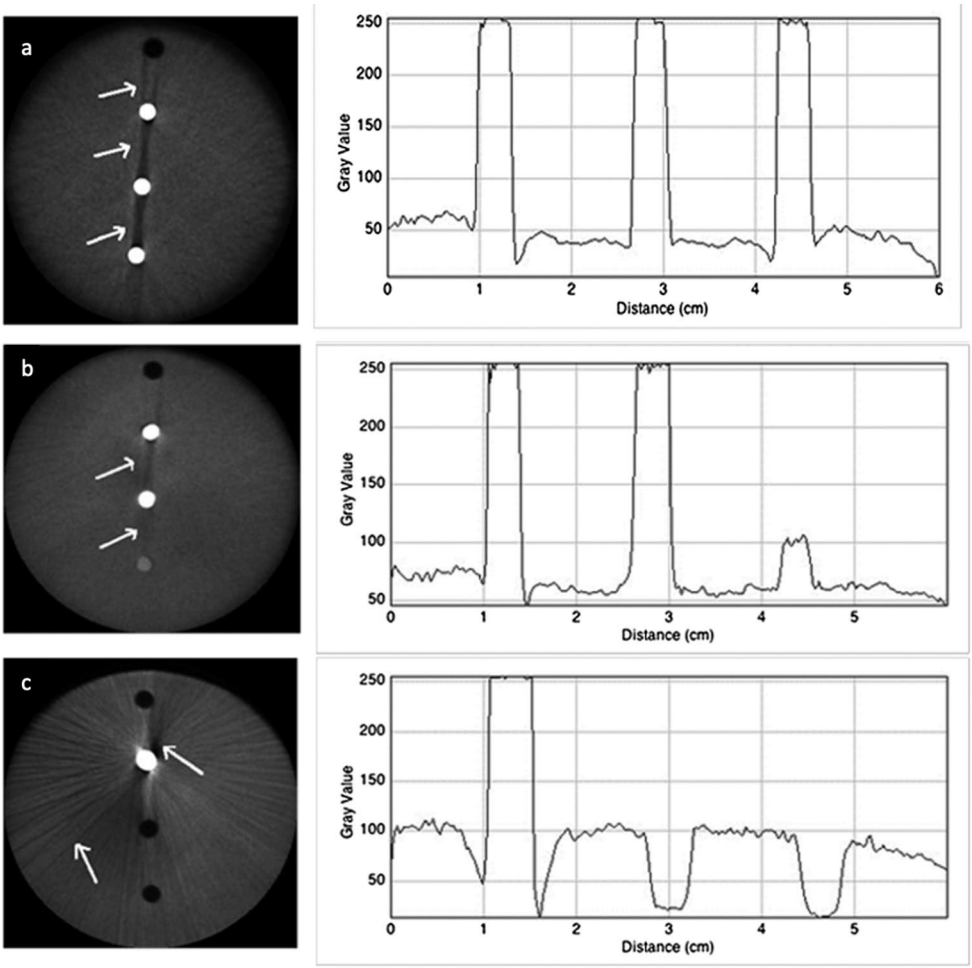

Figure 13. CBCT axial slices and the cross-sections showing gray values. a) Three titanium implant models caused artifacts between the implant models. b) Composite implant models from above 4, 5, 7 caused only moderate artifacts, of which model 7 did not cause artifact. c) Zirconia caused intense artifacts. Modified from the original publication I with permission of DMFR.

In Study II, the titanium implant caused artifacts, negative gray values, in each ROI. Artifacts were seen mostly as dark bands or areas around the implant. Table 4 shows the calculated gray value deviations in the ROIs 1–3 investigated in Study II. Comparison between the gray values without the implant showed that the gray values of the ROIs with the titanium implant were negative in all slices. The mean gray values between the titanium implant and the reference differed the most in the ROI 3, 79.5 units. The FRC implant did not cause any observable artifacts. The gray values of the ROIs with FRC implant and without differed only moderately in each

ROI. The mean gray values between the FRC and the reference differed the most also in the ROI 3, 10.6 units.

Table 4. Calculated mean and standard deviations of the gray values in the ROIs 1–3 with (FRC, Ti) and without (Ref) the implants. Comparison of the mean values was done with an ANOVA test. From the original publication II with permission of DMFR.

	Ref Mean (SD)	*FRC Mean (SD)*	*Ti Mean (SD)*	*P1 FRC vs Ref*	*P2 Ti vs Ref*
ROI 1					
Slice 1	−137.9 (36.7)	−152.3 (35.3)	−150.9 (37.7)	<0.001	<0.001
Slice 2	−131.2 (26.9)	−139.0 (24.2)	−178.5 (67.1)	<0.001	<0.001
Slice 3	−124.9 (26.6)	−130.3 (23.5)	−136.9 (73.1)	<0.001	<0.001
Slice 4	−116.7 (22.9)	−117.4 (20.6)	−138.4 (38.9)	0.502	<0.001
Slice 5	−113.4 (22.5)	−113.1 (20.2)	−129.2 (33.4)	0.764	<0.001
Slice 6	−107.6 (23.0)	−108.0 (20.4)	−123.5 (30.5)	0.668	<0.001
Slice 7	−102.7 (22.1)	−103.8 (22.3)	−120.9 (26.6)	0.153	<0.001
Slice 8	−99.7 (22.5)	−100.7 (20.6)	−117.1 (22.9)	0.190	<0.001
Slice 9	−96.4 (23.3)	−96.8 (20.2)	−109.9 (21.5)	0.740	<0.001
ROI 2					
Slice 1	−250.7 (57.8)	−267.7 (56.5)	−264.0 (58.6)	<0.001[a]	<0.001[a]
Slice 2	−232.7 (55.1)	−243.4 (52.4)	−278.4 (102.7)	<0.001	<0.001
Slice 3	−212.0 (44.5)	−220.4 (47.3)	−277.4 (97.9)	<0.001	<0.001
Slice 4	−176.4 (46.2)	−195.3 (39.6)	−238.9 (114.2)	0.215	<0.001
Slice 5	−165.5 (51.5)	−178.7 (45.9)	−217.0 (108.5)	0.181	<0.001
Slice 6	−165.5 (51.5)	−167.9 (51.1)	−191.9 (90.1)	0.196	<0.001
Slice 7	−159.2 (52.5)	−160.7 (52.9)	−176.6 (69.8)	0.559	<0.001
Slice 8	−155.7 (54.8)	−157.5 (54.0)	−167.6 (56.4)	<0.001[a]	<0.001[a]
Slice 9	−151.1 (52.8)	−153.8 (53.2)	−160.8 (56.0)	0.152	<0.001
ROI 3					
Slice 1	252.3 (448.9)	214.9 (422.1)	150.3 (365.4)	0.086	<0.001
Slice 2	−10.4 (150.5)	−33.9 (137.9)	−156.0 (83.7)	<0.001	<0.001
Slice 3	−79.9 (32.4)	−102.7 (31.6)	−182.1 (116.4)	<0.001	<0.001
Slice 4	−81.8 (31.0)	−81.0 (30.3)	−144.5 (146.8)	0.775	<0.001
Slice 5	−73.6 (21.8)	−71.9 (21,2)	−141.5 (111.9)	0.130	<0.001
Slice 6	−78.4 (19.4)	−80.6 (18.5)	−141.8 (116.1)	0.011	<0.001
Slice 7	−79.4 (19.9)	−80.1 (18.5)	−148.7 (108.2)	0.633	<0.001
Slice 8	−79.5 (24.0)	−83.7 (20.0)	−140.0 (74.8)	<0.001	<0.001
Slice 9	−74.9 (21.2)	−76.6 (16.5)	−116.5 (57.9)	0.087	<0.001

FRC, fibre-reinforced composite group; Ref, reference group; SD, standard deviation; Ti, titanium group.
P1 = significance from Tukey's or Games-Howell's test ([a]Tukey's HSD) FRC *vs* reference.
P2 = significance from Tukey's or Games-Howell's test ([a] Tukey's HSD) Ti *vs* reference.
All the significant (<0.05) *p*-values remained significant after Benjamini-Hochberg's procedure.

5.2.1 CBCT Findings in Study III

The clinical characteristics and the information from the medical reports in Study III are shown in Figure 14. The influence of the artifacts is shown in Figure 15. The overall agreement between the two observers in identifying artifacts is shown in Table 5.

The average age of the patients with CRS was 62 years. Detailed identification of the anatomy at level 1 and the diagnosis of AP were both hampered because of

the artifacts in most of the CBCT images, 97% and 70%, respectively. Artifacts hampered the recognition of the maxillary sinus and the diagnosis of sinusitis in only a few CBCT images, 7.5% and 2.3% respectively. Artifacts did not hamper identifying the anatomy or sinusitis of the paranasal sinuses at level 3.

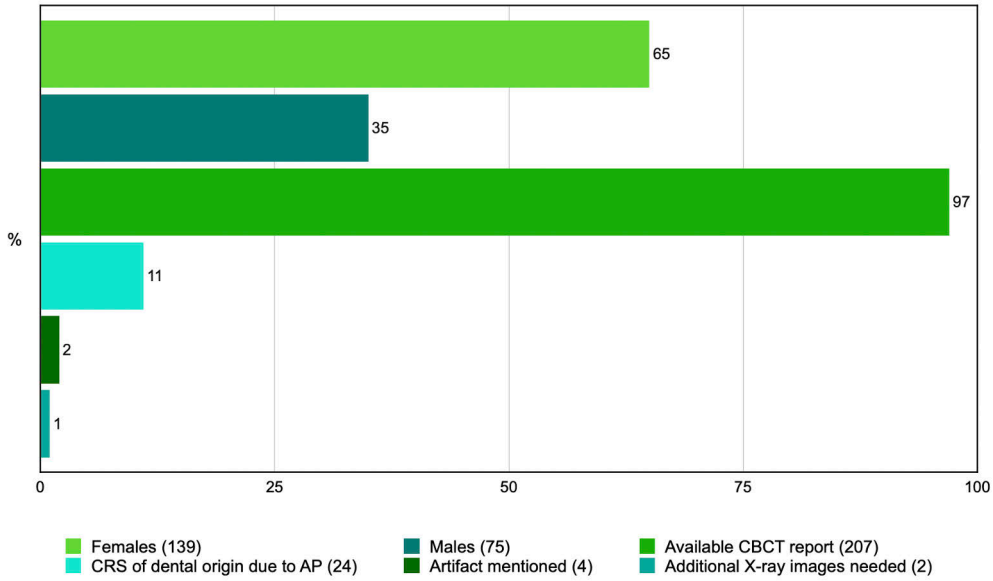

Figure 14. Information of the clinical characteristics and the medical reports of the patients with CRS % (n) in Study III.

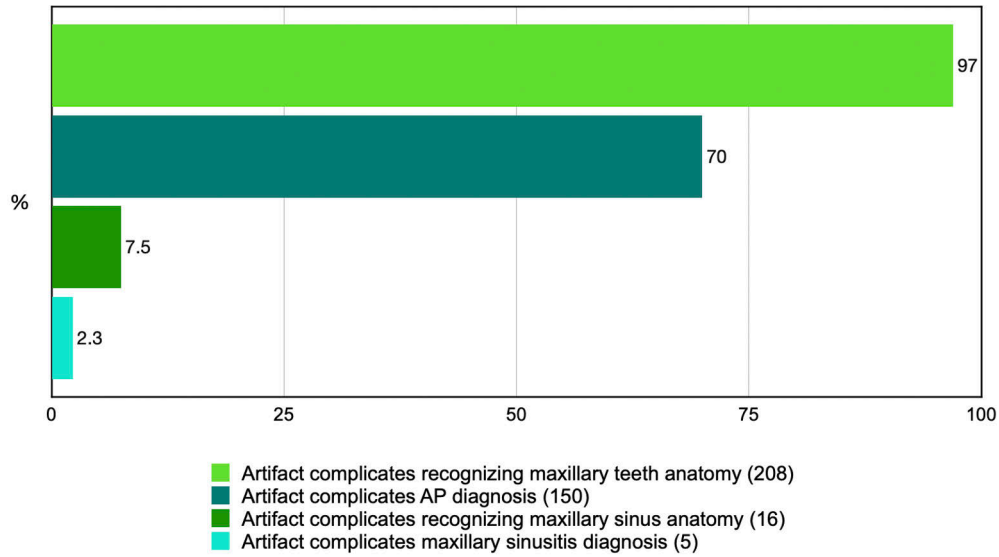

Figure 15. The influence of the artifacts on the diagnosis in the CBCT images % (n) in Study III.

Table 5. The ICC, intra class correlation coefficient test results between observer 1, an oral and maxillofacial radiologist and the interobserver, a head and neck radiologist.

Level in the CBCT image	n/50	ICC test
Level 1	(48/50)	0.960, 95% CI 0.90–1.00
Level 2	(28/50)	0.560, 95% CI 0.42–0.69
Level 3	(47/50)	0.940, 95% CI 0.87–1.00

The most common sources of the artifacts were dental fillings or crowns and endodontic fillings. All the recognized sources are shown in Figure 16. The number of dental implants was low in this study as well as the number of other maxillofacial implants at levels 2 and 3.

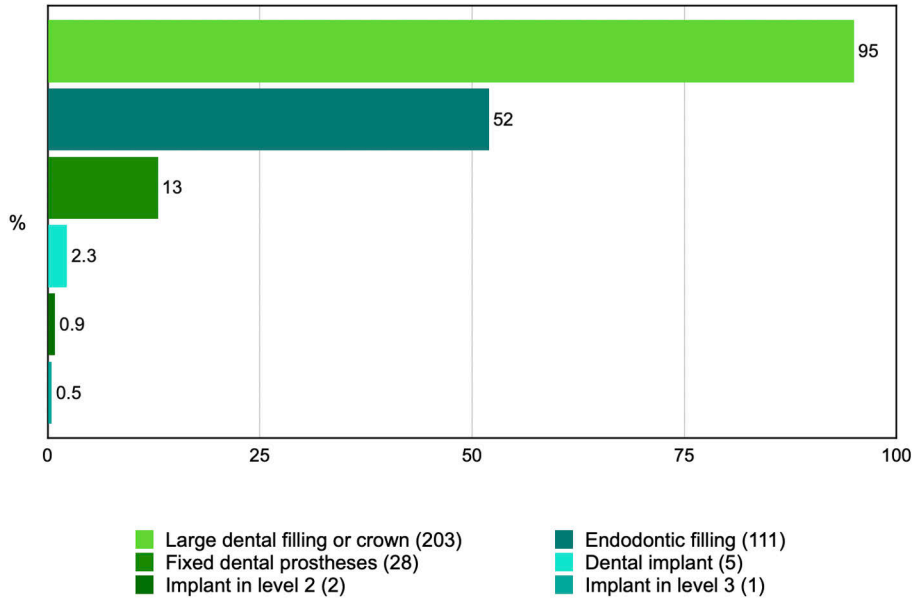

Figure 16. The sources of the artifacts in the CBCT images % (n).

5.2.2 The Function of Artifact Reduction Algorithm ARA

The bone defects of titanium and FRC implants in Study IV were well recognized, with or without ARA. The defect of the zirconia implant could not be identified in any image with or without ARA. The defect measurements and the results of the interobserver agreement are shown in Table 6. The observers equally recognized the marginal cortex, bone structure between the implants and the implant spiral structure. The bone structure or marginal cortex between the zirconia implants could not be recognized even with ARA. The marginal cortex of the titanium and FRC implants was identified in all the images with or without ARA. The bone structure between

the titanium implants was smoother with ARA 2 and ARA 3 with all imaging parameters. The bone structure between the FRC implants was recognized with all imaging parameters with or without ARA. The spiral pattern of the titanium and FRC implants was identified in detail with a resolution of 75 μm with or without ARA.

Table 6. The agreement between the two observers. Modified from the original publication IV with permission of DMFR.

Defect size	Height mm		Width mm		Depth mm		ICC (95%CI)
Observer	1	2	1	2	1	2	
Imaging parameters 1*							
Zirconia no ARA – ARA 3	0	0	0	0	0	0	NA
Titanium no ARA	5.4	5.4	3	3.3	1	1.2	0.998 (0.923–1.000)
ARA 1	6	5.4	2.5	2.1	1.2	0.9	0.991 (0.195–1.000)
ARA 2	5.1	5.1	2.1	1.8	0.9	0.9	0.998 (0.975–1.000)
ARA 3	5.3	5.1	2.4	1.8	1.2	0.6	0.987 (0.210–1.000)
FRC no ARA	5	5.9	2.4	2.4	1.2	1.8	0.977 (0.446–0.999)
ARA 1	5	5.3	2.1	2.7	1.2	1.5	0.988 (0.183–1.000)
ARA 2	5.3	5.9	2.3	2.1	1.2	1.2	0.994 (0.857–1.000)
ARA 3	5.3	6.2	2.2	1.8	1.2	1.2	0.986 (0.588–1.000)
Imaging parameters 2**							
Zirconia no ARA – ARA 3	0	0	0	0	0	0	NA
Titanium no ARA	5.4	5.6	2.7	2.7	0.75	0.8	0.999 (0.988–1.000)
ARA 1	5.1	5.6	2.1	2.1	0.75	0.8	0.996 (0.937–1.000)
ARA 2	5.1	5.3	2.3	2	0.75	0.6	0.998 (0.947–1.000)
ARA 3	5.1	5.3	2.3	2	0.75	0.8	0.998 (0.916–1.000)
FRC no ARA	5.3	6.1	2.7	2.1	1	1.2	0.984 (0.420–1.000)
ARA 1	5.3	5.9	2.7	2.9	1	1.3	0.992 (0.441–1.000)
ARA 2	5.3	5.9	2.7	2.9	1	1.2	0.993 (0.626–1.000)
ARA 3	5.3	5.8	2.7	3	1	1.2	0.995 (0.990–0.998)
Imaging parameters 3***							
Zirconia no ARA – ARA 3	0	0	0	0	0	0	NA
Titanium no ARA	5.4	5.6	2.7	2.7	0.75	0.8	0.999 (0.988–1.000)
ARA 1	5.1	5.6	2.1	2.1	0.75	0.8	0.996 (0.937–1.000)
ARA 2	5.1	5.3	2.3	2	0.75	0.6	0.998 (0.947–1.000)
ARA 3	5.1	5.3	2.3	2	0.75	0.8	0.998 (0.916–1.000)
FRC no ARA	5.3	6.1	2.7	2.1	1	1.2	0.984 (0.420–1.000)
ARA 1	5.3	5.9	2.7	2.9	1	1.3	0.992 (0.441–1.000)
ARA 2	5.3	5.9	2.7	2.9	1	1.2	0.993 (0.626–1.000)
ARA 3	5.3	5.8	2.7	3	1	1.2	0.995 (0.990–0.998)

* Whole mandible, FOV 22 x 12 cm, 100 kV, 12 mA, 5 s with a resolution of 300 μm ** The implant pairs, FOV 5 x 5 cm, 90 kV, 14 mA, 4.5 s with a resolution of 150 μm *** The implant pairs, FOV 5 x 5 cm, 100kV, 12 mA, 12.8 s with a resolution of 75 μm.

NA, not applicable; ICC, intra class correlation coefficient; observer 1, oral and maxillofacial radiologist; observer 2 bachelor of dental sciences; ARA, artifact reduction algorithm of Planmeca Viso G7; FRC, fiber reinforced composite

6 Discussion

6.1 The Development of the CBCT Devices

During the last 20 years, CBCTs have become an essential part of the diagnosis of many kinds of dental and maxillofacial disorders. Around 279 different CBCT models are currently available with different technical features (Gaêta-Araujo et al., 2021). Because of the wide variety of the CBCT models and the imaging parameters used, the results acquired from different studies, especially from in vitro studies, should not be taken directly into clinical use or generalized (Gaêta-Araujo et al., 2020). The studies in this thesis were mainly experimental (I, II, IV), in which different restoration and implant materials were easily and quickly compared to each other. However, CBCT models and their performance should be considered individually and the study results cannot be directly compared with those achieved with other CBCT models (Gaêta-Araujo et al., 2021). In the studies in this thesis, four different CBCT devices were used during the years 2014–2022, all of which represent different technical features and versions during this time. One is no longer available on the market, the SCANORA 3D (Soredex, Tuusula, Finland), and another is one of the latest CBCT devices available, Plameca Viso G7 (Planmeca, Helsinki, Finland). Hence, the results of these studies are not fully comparable.

6.1.1 CBCT Indications

Due to the advances in CBCT equipment and research, a revision of the recommendations and the clinical guidelines of CBCT imaging has been demanded (Gaêta-Araujo et al., 2021). Endodontic indications for CBCT imaging, such as periapical diseases, are mentioned in the guidelines of SEDENTEXCT. Presently, the National German guidelines for CBCT imaging is the only one covering the pathologies of the paranasal sinuses. Apical periodontitis is diagnosed primarily with intraoral images, but CBCT imaging is indicated in complex situations and, for example, when there is a suspicion of it being the source of CRS. In Study III, we evaluated the CBCT images of paranasal sinuses with an indication of CRS. AP was suspected to be the origin of CRS in 11% of cases. The diagnosis of AP and CRS needs a careful clinical evaluation, and the radiological examinations should be considered individually.

In addition, CBCT is established as an accurate method for preoperative implant placement, but because of the artifacts induced by implants, CBCT should not be used postoperatively (Kim et al., 2020). Peri-implantitis is a growing disorder as implant placements are popular worldwide. The diagnosis of peri-implantitis, however, is recommended to be primarily performed with a clinical evaluation and conventional radiographs (Jacobs et al., 2018). CBCT should be considered only for specific cases, such as sensory problems (Kim et al., 2020). In the experimental study this thesis, Study IV, the indication for CBCT imaging was a complicated peri-implantitis with a defect. Recommendations for postoperative CBCT imaging, especially in cases of peri-implantitis, are needed in future.

6.1.2 CBCT Imaging Parameters and MAR Algorithms

The imaging parameters were only tested in Study IV, which was also the only study with an artifact reduction algorithm. Image quality improving algorithms are individual features of the CBCT devices. In Study IV, the spiral structure of the implants was only identified with a resolution of 75 µm and with the smaller FOV 5 × 5 cm. Image sharpness can be achieved with the smaller voxel sizes, but the noise will be increased (Pauwels, Araki, et al., 2015). It is always recommended to keep the FOV as small as possible to reduce the radiation dose (Pauwels, Araki, et al., 2015). Schriber and coworkers found that the low-dose and high-dose CBCT parameters only had a small influence on the artifacts (Schriber et al., 2020). Also, Nomier and coworkers suggest the low-dose CBCT imaging for evaluating the peri-implant bone (Nomier et al., 2022). In these studies, however, there was only one implant imaged.

Although MAR algorithms reduce artifacts, their performance is influenced by different CBCT devices, materials and FOV sizes (Vasconcelos et al., 2019). Some studies advocate the use of MAR in specific CBCT devices (de Faria Vasconcelos et al., 2020), especially when the artifacts are more pronounced (Fontenele et al., 2020). In specific diagnostic tasks, such as internal root resorption, studies show that MAR is effective if artifacts are present (Gaêta-Araujo et al., 2020). The meta-analysis of Fontenele and coworkers demonstrated that a vertical root fracture could be diagnosed better without MAR (Fontenele, Machado, et al., 2021). In addition, when detecting a vertical root fracture near a zirconium implant, MAR activation is inefficient (Fontenele, Farias Gomes, et al., 2021). MAR activation and an increase in kVp are shown to decrease the artifacts (Freitas et al., 2018). Moreover, an increased tube current and MAR activation improve the image quality when zirconia implants are present (Mancini et al., 2021). The studies of Sheikhi and coworkers and Salemi and coworkers do not recommend the use of MAR in evaluating peri-implant bone defects (Salemi, 2021; Sheikhi et al., 2020).

Only one CBCT device with the MAR method was used in this thesis. Thus, it is not possible to provide a recommendation for its use based on this one experiment. Similarly, Gaêta-Araujo and coworkers concluded that, material and patient related CBCT artifacts should be considered with caution because most studies are mainly *in vitro* studies with phantoms and performed with different CBCT devices (Gaêta-Araujo et al., 2021). In Study IV, we noticed that a metal artifact reduction algorithm is unnecessary for diagnosing peri-implant bone around titanium and FRC dental implants.

Currently, additional means to reduce the artifacts in the CBCT images other than MAR methods are scarce. The results of the studies of Luckow et al., 2011 and Min et al., 2021 encourage tilting a patient's head to reduce metal artifacts in CBCT images (Luckow et al., 2011; Min & Kim, 2021b). This is also mentioned in the SEDENTEXCT guidelines to reduce artifacts induced by dental restorations (Radiation Protection 172, 2012).

However, another study by Min & Kim 2021 highlights that the effect of tilting depends on the location of the implants (Min & Kim, 2021a). Furthermore, in current scanners the head is fixed in a certain position, and there may be limited space for head tilting (Min & Kim, 2021a).

6.1.3 Artifacts in the CBCT Images

In Studies I, II, and IV, we showed the detrimental effects of titanium dental implants and orbital floor implants in the CBCT images. Studies I and IV also showed the detrimental effects of zirconia dental implants. Because of the growing popularity of zirconia as an implant and crown material, the detrimental effects in the postoperative CBCT images should be taken in account beforehand. The present Studies I and IV showed that artifacts caused by zirconia were clearly more intense than those caused by titanium. This result agrees with the recent study of Warren and coworkers (Warren et al., 2022). This difference is explained by the high atomic number of the main component (R. Schulze, 2022). Moreover, the intensity of artifacts is multipled when several implants are set side by side, which is currently quite common (I, IV).

Composite based FRC orbital floor implants do not cause intense artifacts, as shown in Study II. The result of this study implies that FRC implants could be used in cases where postoperative CBCT monitoring is necessary. Similarly, we found in Study IV that dental implant models made of FRC did not cause detrimental artifacts in the CBCT images and the bone around the implants were well recognized. Hence, FRC as a dental implant material would be beneficial especially in the areas of thin alveolar bone. In turn, Study I showed that composites including $BaAlSiO_2$ 20%

(wt%) or more can cause artifacts in CBCT images and composites $BaAlSiO_2$ 68% (wt%) or more can lead to artifacts as intense as the titanium's (I).

In Study III, most of the artifacts seen in the CBCT images originated from large dental and endodontic restorations. Although the diagnosis of sinusitis was not hampered in the CBCT images, the diagnosis of AP was hampered in 70% of the cases. This may lead to an incorrect etiology of CRS and further, to inappropriate or excessive treatments and medication.

In Study III, we investigated only the origins of the artifacts located in the FOV. Motion artifacts were not evaluated in this thesis, nor materials located in the exomass that can also cause artifacts in the CBCT image (Andrade-Bortoletto et al., 2023; Demirturk Kocasarac et al., 2022). Also, the size of the object has influence on the artifact expression. Moshfeghi and coworkers found out that artifacts are more pronounced when the object is larger than the FOV (Moshfeghi et al., 2022). Importantly, we noticed in Study III, that the CBCT reports usually lacked to note the presence of the artifacts (4/214). In the SEDENTEXCT guidelines, however, artifacts are mentioned in the list for radiological interpretation (Radiation Protection 172, 2012). In Study III, we also highlighted the importance to note the artifacts in the report, because clinicians may not be as familiar with the artifacts and their disturbing effects on the CBCT image interpretation and the consequences it causes. We also found in Study III that the CBCT reports did not include recommendations for additional X-ray images, such as intraoral images, despite the image hampering artifacts as shown in Figures 17 and 18.

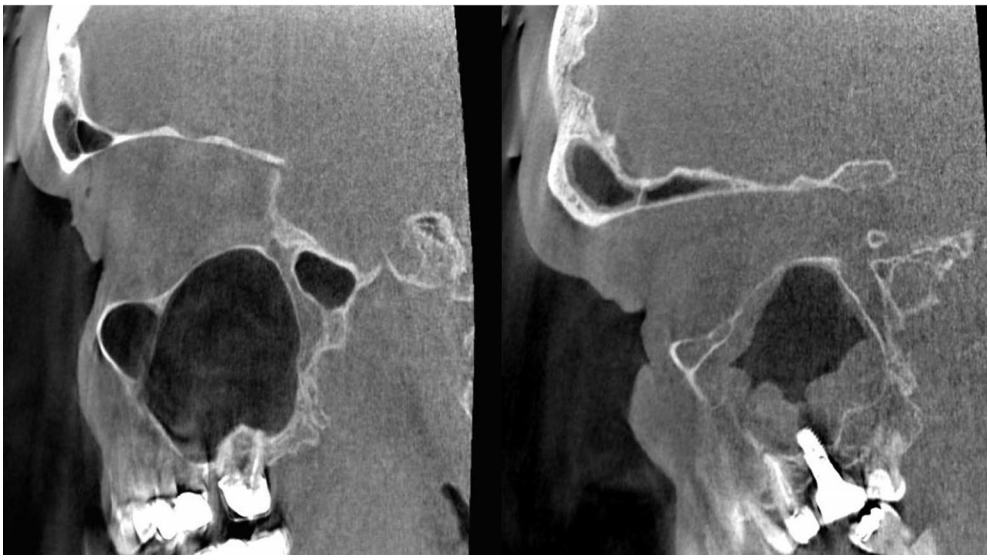

Figure 17. Two sagittal views of paranasal sinus CBCT images showing artifacts due to crowns and a dental implant (right). Mucosal thickening is easily recognized on the right.

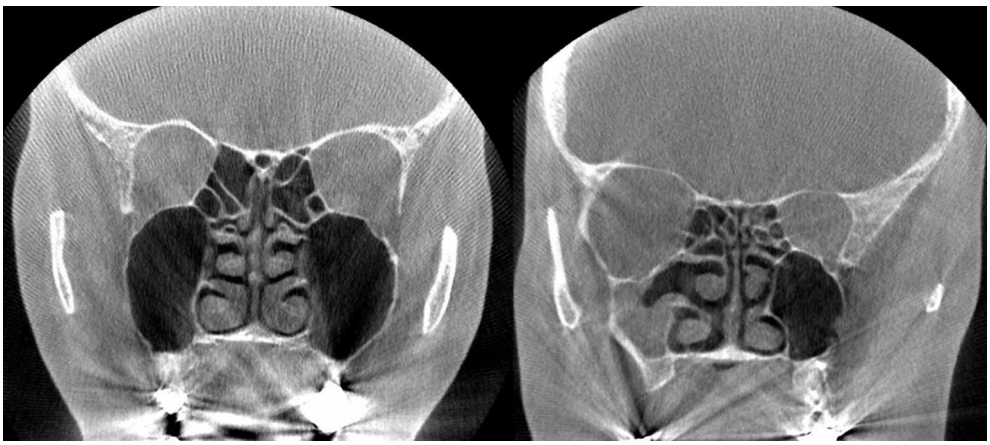

Figure 18. Two coronal views of paranasal sinus CBCT images showing detrimental artifacts due to crowns. Periapical areas of the maxillary molars are not reliably recognized.

6.2 Image Analysis

In Studies III and IV, we had two observers with different backgrounds and experiences for image analysis. Expertise and experience are essential when diagnosing challenging cases, like apical periodontitis and peri-implantitis. In Study III, the overall agreement to identify artifacts was substantial to almost perfect (Table 6.), and in Study IV for all categories, the interobserver agreement was almost perfect (Table 7). However, the image analysis of these studies is done in a calm and quiet circumstance without disturbing factors such as hurry or interruptions. This does not equate to the clinical circumstances; these factors may influence the image analysis and diagnosis (Hegde et al., 2023).

In Studies I and II, we used the gray values of the CBCT images to demonstrate and to compare the intensity of artifacts. However, it is known, that the gray values of the CBCT should not be used in diagnosing because of its unreliability, especially when artifacts are present (Pauwels, Jacobs, et al., 2015).

In addition, STUK has recently provided recommendations for the diagnostic monitors (Heikkilä et al. 2022). Monitors of 3 megapixels can represent CT, CBCT and MRI images at their original resolution. The monitor used in Studies III and IV was with 3 megapixels which agrees the minimum requirement for diagnostic monitors.

6.3 Limits and Prospects

In this thesis, three out of four studies (I, II, IV) were experimental studies. These kinds of studies are quick and more effortless to perform because of lighter study permissions. However, phantoms and study sets used in these studies do not fully

correlate with the real cases because of absent soft tissues and other anatomic structures that may impact the artifact appearance in the CBCT images. Although the results of the in vitro studies do not correspond to the clinical situations, phantom studies are an important base for further clinical studies.

At the moment, there is a need for further studies with several CBCT models and studies of diagnostic and treatment efficacy (Gaêta-Araujo et al., 2020). MAR methods with different materials and different numbers of materials should be studied further to understand their function. In future, it would be important to have device specific recommendations and conclusions of the use of MAR in future. Yet, it is unclear, whether MAR methods just improve the image quality or aid to diagnose and recognize the anatomy.

Radiation dose monitoring was not the topic of these studies. However, dentists use X-ray images and CBCT images at a large scale with children and young adults. Hence, there is a special need for justification and optimization. The current CBCT guidelines do not provide recommendations for postoperative CBCT imaging. According to the results of the studies of this thesis, postoperative CBCT imaging on patients with zirconia implants or multiple implants may be reasonable to avoid because of the image hampering artifacts. In these cases, the overall value and benefit of the CBCT image should be reconsidered carefully. In future, a caution of zirconia related artifacts in postoperative CBCT imaging may be worth to include in the updated CBCT guidelines.

In the future, image analysis will be facilitated by artificial intelligence (AI). For example, the study by Minnema et al. 2019 showed that a deep learning algorithm can accurately segment teeth and bony structures in CBCT scans despite the metal artifacts (Minnema et al., 2019). The diagnosis of complicated cases in the CBCT images needs the expertise and experience of the observer, but detrimental artifact is a factor that impair the subjective image analysis. In challenging cases, AI solutions are going to be a necessary tool in image analysis.

7 Conclusions

The present studies showed the differences between dental and maxillofacial restoration materials to generate artifacts in the CBCT images. Nonmetallic material options, such as composite based materials, could be considered when postoperative CBCT images are needed. Artifact reduction algorithms need to be improved to achieve a diagnostically better image quality especially when zirconia-based materials are present.

The main conclusions are:

- Composites including $BaAlSiO_2$ 20% (weight%) or more can cause artifacts in the CBCT images while composites including $BaAlSiO_2$ 68% (weight%) or more cause artifacts as intense as titanium.
- Zirconia causes the most intense artifacts in CBCT images of the investigated materials. Titanium causes artifacts in CBCT images, especially when multiple implants are present.
- FRC orbital floor implant does not cause detrimental artifacts in the CBCT images. Titanium orbital floor implant causes artifacts in the CBCT images.
- The diagnosis of AP can be complicated in 70% of the CBCT images of paranasal sinuses because of artifacts that can lead to misdiagnosis between CRS and CRS with a dental origin.
- Peri-implant bone or peri-implant bone defect cannot be diagnosed around two side by side zirconia implants despite the metal artifact reduction algorithm. Metal artifact reduction algorithm is not necessary for diagnosing peri-implant bone around titanium and FRC implants.

Acknowledgements

This thesis was carried out in the Department of Oral Pathology and Radiology at the Institute of Dentistry, University of Turku, and Turku Clinical Biomaterials Centre (TCBC), during the years 2014–2023. Personal grants were received from the Finnish Dental Society Apollonia, the Finnish Association of Women Dentists, and Lapuan Naisyhdistys ry. The financial support is greatly appreciated.

I would like to warmly thank my supervisor, Professor Sisko Huumonen. Thank you for your guidance and encouragement through these years. My deepest thanks also go to my second supervisor, Dean of the Institute of Dentistry, Professor Pekka Vallittu. Your inspiring and positive attitude is communicated to everyone around you. I would also like to express my sincere thanks to my third supervisor, Professor Emerita Stina Syrjänen. I admire your attitude to work. Thank you for helping me to solve problems, both the major and the minor ones.

I want to thank Docent Michaela Bode for accepting the invitation to be my opponent at the defense of this thesis. The reviewers, Professor Reinhilde Jacobs and Associate Professor Jaakko Sarin, are greatly acknowledged for their valuable work in improving this thesis.

Especial thanks to my co-authors, head of the laboratory at TCBC Lippo Lassila, MSc, PhD Antti Kotiaho, MSc, PhD Marianne Haapea, MD, PhD Jami Rekola, Professor Jussi Hirvonen, MSc Auli Suominen, Professor Ilpo Kinnunen, DDS, PhD Faleh Abushahba, and Professor Timo Närhi for careful and critical work. I learned a lot from your comments and opinions, and it is always a pleasure to cooperate with people with different specialties.

I want to thank the staff at the Institute of Dentistry and TCBC during the years 2014-2023. I also warmly thank Ari Hietanen from Planmeca for cooperating with me in Study IV. I warmly thank Elizabeth Nyman for the language check of the articles and the thesis. Thank you for always being kind and helpful. I also want to thank my previous and present managers at the Central Hospital of Päijät-Häme, MD Auli Malinen and MD Mikko Jousi, for being flexible and understanding during this project.

I warmly thank my colleagues at the Department of Oral Pathology and Radiology, Professor Jaana Hagström, DDS, PhD Jaana Willberg, DDS Katariina

Piiparinen, DDS Katri Aantaa and my roommate in Dentalia, Professor Emerita Eva Söderling. Thank you for productive and supportive discussions. Also, I would like to thank my colleagues and dear friends elsewhere – Antti Lehtinen, Krista Vasankari, Nina Sjöberg, Helena Mehtonen, and Essi Nikkanen. Thank you for being supportive and sympathetic. Susanna and Olli Likitalo, thank you for supportive discussions. In future, let's attend the Ceremonial Conferment together. In addition, Anni and Henri Honka, thank you for the deep and entertaining conversations about life!

Above all, I want to thank my dear husband, Martti Merikari. You have certainly had the most important job standing beside me every day during this project. You are always helpful, encouraging, and compassionate. I sincerely thank my parents, Marketta and Yrjö Kuusisto, and my sister Marianne Kuusisto. You, my family, have undoubtedly supported my decisions in life.

I am privileged to have the opportunities and possibilities to educate and improve myself as a radiologist and a researcher. Hence, I would like to thank my dear grandparents in heaven.

Turku, August 2023
Niina Kuusisto

References

Abdulmajeed, A. A., Närhi, T. O., Vallittu, P. K., & Lassila, L. V. (2011). The effect of high fiber fraction on some mechanical properties of unidirectional glass fiber-reinforced composite. *Dental Materials*, *27*(4), 313–321. https://doi.org/10.1016/j.dental.2010.11.007

Agrawal, A. A., & Chitko, S. S. (2011). The use of silane-coated industrial glass fibers in splinting periodontally mobile teeth. *Indian Journal of Dental Research: Official Publication of Indian Society for Dental Research*, *22*(4), 594–596. https://doi.org/10.4103/0970-9290.90307

Aitasalo, K. M. J., Piitulainen, J. M., Rekola, J., & Vallittu, P. K. (2014). Craniofacial bone reconstruction with bioactive fiber-reinforced composite implant: Bioactive Fiber-Reinforced Composite Implant. *Head & Neck*, *36*(5), 722–728. https://doi.org/10.1002/hed.23370

Akalın-Evren, B., Kulak-Özkan, Y., Ozcan, M., & Kadir, T. (2014). Candida albicans adhesion on reinforced polymethylmethacrylate denture resin: Effect of fibre architecture and exposure to saliva. *Gerodontology*, *31*(3), 194–201. https://doi.org/10.1111/ger.12024

Amarnath, G., Muddugangadhar, B., Tripathi, S., Dikshit, S., & Ms, D. (2011). Biomaterials for Dental Implants: An Overview. *International Journal of Oral Implantology & Clinical Research*, *2*(1), 13–24. https://doi.org/10.5005/jp-journals-10012-1030

Andrade-Bortoletto, M. F. S., Fontenele, R. C., Farias-Gomes, A., & Freitas, D. Q. (2023). Mapping artifacts generated in a tooth adjacent to titanium and zirconia implants located in the endomass and exomass in cone beam computed tomography: An ex vivo study. *Oral Surgery, Oral Medicine, Oral Pathology and Oral Radiology*, S2212440323006132. https://doi.org/10.1016/j.oooo.2023.08.002

Angelopoulos, C., Scarfe, W. C., & Farman, A. G. (2012). A Comparison of Maxillofacial CBCT and Medical CT. *Atlas of the Oral and Maxillofacial Surgery Clinics*, *20*(1), 1–17. https://doi.org/10.1016/j.cxom.2011.12.008

Bal, M., & Spies, L. (2006). Metal artifact reduction in CT using tissue-class modeling and adaptive prefiltering: Metal artifact reduction in CT. *Medical Physics*, *33*(8), 2852–2859. https://doi.org/10.1118/1.2218062

Bayat, S., Talaeipour, A. R., & Sarlati, F. (2016). Detection of simulated periodontal defects using cone-beam CT and digital intraoral radiography. *Dentomaxillofacial Radiology*, *45*(6), 20160030. https://doi.org/10.1259/dmfr.20160030

Benic, G. I., Sancho-Puchades, M., Jung, R. E., Deyhle, H., & Hämmerle, C. H. F. (2013). *In vitro* assessment of artifacts induced by titanium dental implants in cone beam computed tomography. *Clinical Oral Implants Research*, *24*(4), 378–383. https://doi.org/10.1111/clr.12048

Bijelic-Donova, J., Garoushi, S., Lassila, L. V. J., & Vallittu, P. K. (2015). Oxygen inhibition layer of composite resins: Effects of layer thickness and surface layer treatment on the interlayer bond strength. *European Journal of Oral Sciences*, *123*(1), 53–60. https://doi.org/10.1111/eos.12167

Butterworth, C., Ellakwa, A. E., & Shortall, A. (2003). Fibre-reinforced composites in restorative dentistry. *Dental Update*, *30*(6), 300–306. https://doi.org/10.12968/denu.2003.30.6.300

Cacciafesta, V., Sfondrini, M. F., Lena, A., Scribante, A., Vallittu, P. K., & Lassila, L. V. (2007). Flexural strengths of fiber-reinforced composites polymerized with conventional light-curing and additional postcuring. *American Journal of Orthodontics and Dentofacial Orthopedics: Official*

Publication of the American Association of Orthodontists, Its Constituent Societies, and the American Board of Orthodontics, *132*(4), 524–527. https://doi.org/10.1016/j.ajodo.2005.09.036

Casselman, J., & Gieraerts, K. (n.d.). *CONE BEAM CT: NON-DENTAL APPLICATIONS*.

Christiaens, V., De Bruyn, H., De Vree, H., Lamoral, S., Jacobs, R., & Cosyn, J. (2018). A controlled study on the accuracy and precision of intraoral radiography in assessing interproximal bone defect morphology around teeth and implants. *European Journal of Oral Implantology*, *11*(3), 361–367.

Cionca, N., Hashim, D., & Mombelli, A. (2017). Zirconia dental implants: Where are we now, and where are we heading? *Periodontology 2000*, *73*(1), 241–258. https://doi.org/10.1111/prd.12180

Codari, M., de Faria Vasconcelos, K., Ferreira Pinheiro Nicolielo, L., Haiter Neto, F., & Jacobs, R. (2017). Quantitative evaluation of metal artifacts using different CBCT devices, high-density materials and field of views. *Clinical Oral Implants Research*, *28*(12), 1509–1514. https://doi.org/10.1111/clr.13019

Comisso, I., Arias-Herrera, S., & Gupta, S. (2021). Zirconium dioxide implants as an alternative to titanium: A systematic review. *Journal of Clinical and Experimental Dentistry*, e511–e519. https://doi.org/10.4317/jced.58063

de Faria Vasconcelos, K., Queiroz, P. M., Codari, M., Pinheiro Nicolielo, L. F., Freitas, D. Q., Jacobs, R., & Haiter-Neto, F. (2020). A quantitative analysis of metal artifact reduction algorithm performance in volume correction with 3 CBCT devices. *Oral Surgery, Oral Medicine, Oral Pathology and Oral Radiology*, *130*(3), 328–335. https://doi.org/10.1016/j.oooo.2020.03.049

De Man, B., Nuyts, J., Dupont, P., Marchal, G., & Suetens, P. (1999). Metal streak artifacts in X-ray computed tomography: A simulation study. *IEEE Transactions on Nuclear Science*, *46*(3), 691–696. https://doi.org/10.1109/23.775600

Demirturk Kocasarac, H., Koenig, L. J., Ustaoglu, G., Oliveira, M. L., & Freitas, D. Q. (2022). CBCT image artefacts generated by implants located inside the field of view or in the exomass. *Dentomaxillofacial Radiology*, *51*(2), 20210092. https://doi.org/10.1259/dmfr.20210092

Derks, J., & Tomasi, C. (2015). Peri-implant health and disease. A systematic review of current epidemiology. *Journal of Clinical Periodontology*, *42*, S158–S171. https://doi.org/10.1111/jcpe.12334

Eldib, M. E., Hegazy, M. A. A., Cho, M. H., Cho, M. H., & Lee, S. Y. (2018). A motion artifact reduction method for dental CT based on subpixel-resolution image registration of projection data. *Computers in Biology and Medicine*, *103*, 232–243. https://doi.org/10.1016/j.compbiomed.2018.10.028

Feldkamp LA, Davis LC, & Kress JW. (n.d.). Practical cone-beam algorithm. *Opt. Soc. Am.*, *1984*(A/Vol. 1, No. 6/June).

Foek, D. L. S., Yetkiner, E., & Ozcan, M. (2013). Fatigue resistance, debonding force, and failure type of fiber-reinforced composite, polyethylene ribbon-reinforced, and braided stainless steel wire lingual retainers in vitro. *Korean Journal of Orthodontics*, *43*(4), 186–192. https://doi.org/10.4041/kjod.2013.43.4.186

Fontenele, R. C., Farias Gomes, A., Nejaim, Y., & Freitas, D. Q. (2021). Do the tube current and metal artifact reduction influence the diagnosis of vertical root fracture in a tooth positioned in the vicinity of a zirconium implant? A CBCT study. *Clinical Oral Investigations*, *25*(4), 2229–2235. https://doi.org/10.1007/s00784-020-03538-4

Fontenele, R. C., Machado, A. H., De Oliveira Reis, L., & Freitas, D. Q. (2021). Influence of metal artefact reduction tool on the detection of vertical root fractures involving teeth with intracanal materials in cone beam computed tomography images: A systematic review and meta-analysis. *International Endodontic Journal*, *54*(10), 1769–1781. https://doi.org/10.1111/iej.13569

Fontenele, R. C., Nascimento, E. H. L., Santaella, G. M., & Freitas, D. Q. (2020). Does the metal artifact reduction algorithm activation mode influence the magnitude of artifacts in CBCT images? *Imaging Science in Dentistry*, *50*(1), 23–30. https://doi.org/10.5624/isd.2020.50.1.23

Freitas, D. Q., Fontenele, R. C., Nascimento, E. H. L., Vasconcelos, T. V., & Noujeim, M. (2018). Influence of acquisition parameters on the magnitude of cone beam computed tomography artifacts. *Dentomaxillofacial Radiology*, *47*(8), 20180151. https://doi.org/10.1259/dmfr.20180151

Gaêta-Araujo, H., Alzoubi, T., Vasconcelos, K. de F., Orhan, K., Pauwels, R., Casselman, J. W., & Jacobs, R. (2020). Cone beam computed tomography in dentomaxillofacial radiology: A two-decade overview. *Dentomaxillofacial Radiology*, *49*(8), 20200145. https://doi.org/10.1259/dmfr.20200145

Gaêta-Araujo, H., Leite, A. F., Vasconcelos, K. de F., & Jacobs, R. (2021). Two decades of research on CBCT imaging in DMFR – an appraisal of scientific evidence. *Dentomaxillofacial Radiology*, *50*(4), 20200367. https://doi.org/10.1259/dmfr.20200367

Gaêta-Araujo, H., Nascimento, E. H. L., Oliveira-Santos, N., Pinheiro, M. C. R., Coelho-Silva, F., & Oliveira-Santos, C. (2020). Influence of adjacent teeth restored with metal posts in the detection of simulated internal root resorption using CBCT. *International Endodontic Journal*, *53*(9), 1299–1306. https://doi.org/10.1111/iej.13348

Garoushi, S. K., Lassila, L. V. J., Tezvergil, A., & Vallittu, P. K. (2006). Fiber-reinforced composite substructure: Load-bearing capacity of an onlay restoration and flexural properties of the material. *The Journal of Contemporary Dental Practice*, *7*(4), 1–8.

Garoushi, S. K., Lassila, L. V. J., & Vallittu, P. K. (2006). Short fiber reinforced composite: The effect of fiber length and volume fraction. *The Journal of Contemporary Dental Practice*, *7*(5), 10–17.

Garoushi, S., Vallittu, P. K., & Lassila, L. V. J. (2008). Depth of cure and surface microhardness of experimental short fiber-reinforced composite. *Acta Odontologica Scandinavica*, *66*(1), 38–42. https://doi.org/10.1080/00016350801918377

Goulston, R., Davies, J., Horner, K., & Murphy, F. (2016). Dose optimization by altering the operating potential and tube current exposure time product in dental cone beam CT: A systematic review. *Dentomaxillofacial Radiology*, *45*(3), 20150254. https://doi.org/10.1259/dmfr.20150254

Hegde, S., Gao, J., Vasa, R., & Cox, S. (2023). Factors affecting interpretation of dental radiographs. *Dentomaxillofacial Radiology*, *52*(2), 20220279. https://doi.org/10.1259/dmfr.20220279

Heikkilä, Janne; Hippeläinen, Eero; Kallio-Pulkkinen, Soili; Lajunen, Atte; Lepola, Pasi; Liukkonen, Esa; Nieminen, Miika; Peuna, Arttu; Sierpowska, Joanna; Vitikainen, Anne-Mari. (2022). *Suositus kuvankatselunäytöille ja niiden laadunvalvontaan*. STUK opastaa. https://urn.fi/URN:ISBN:978-952-309-546-5

Hsieh, J. (2003). *Computed tomography: Principles, design, artifacts, and recent advances*. SPIE Optical Engineering Press.

Jacobs, R. (2011). Dental cone beam ct and its justified use in oral health care. *Journal of the Belgian Society of Radiology*, *94*(5), 254. https://doi.org/10.5334/jbr-btr.662

Jacobs, R., Vranckx, M., Vanderstuyft, T., Quirynen, M., & Salmon, B. (2018). CBCT vs other imaging modalities to assess peri-implant bone and diagnose complications: A systematic review. *European Journal of Oral Implantology*, *11 Suppl 1*, 77–92.

Kalender, W. A., Hebel, R., & Ebersberger, J. (1987). Reduction of CT artifacts caused by metallic implants. *Radiology*, *164*(2), 576–577. https://doi.org/10.1148/radiology.164.2.3602406

Kiljunen, T., Kaasalainen, T., Suomalainen, A., & Kortesniemi, M. (2015). Dental cone beam CT: A review. *Physica Medica*, *31*(8), 844–860. https://doi.org/10.1016/j.ejmp.2015.09.004

Kim, M.-J., Lee, S.-S., Choi, M., Yong, H. S., Lee, C., Kim, J.-E., & Heo, M.-S. (2020). Developing evidence-based clinical imaging guidelines of justification for radiographic examination after dental implant installation. *BMC Medical Imaging*, *20*(1), 102. https://doi.org/10.1186/s12880-020-00501-3

Kumbuloglu, O., Ozcan, M., & User, A. (2008). Fracture strength of direct surface-retained fixed partial dentures: Effect of fiber reinforcement versus the use of particulate filler composites only. *Dental Materials Journal*, *27*(2), 195–202. https://doi.org/10.4012/dmj.27.195

Kuusisto, N., Vallittu, P. K., Lassila, L. V. J., & Huumonen, S. (2015). Evaluation of intensity of artefacts in CBCT by radio-opacity of composite simulation models of implants *in vitro*. *Dentomaxillofacial Radiology*, *44*(2), 20140157. https://doi.org/10.1259/dmfr.20140157

Ladizesky, N. H., Chow, T. W., & Cheng, Y. Y. (1994). Denture base reinforcement using woven polyethylene fiber. *The International Journal of Prosthodontics*, *7*(4), 307–314.

Lassila, L. V. J., Tanner, J., Le Bell, A.-M., Narva, K., & Vallittu, P. K. (2004). Flexural properties of fiber reinforced root canal posts. *Dental Materials: Official Publication of the Academy of Dental Materials*, *20*(1), 29–36. https://doi.org/10.1016/s0109-5641(03)00065-4

Lazar, M.-A., Rotaru, H., Bâldea, I., Boşca, A. B., Berce, C. P., Prejmerean, C., Prodan, D., & Câmpian, R. S. (2016). Evaluation of the Biocompatibility of New Fiber-Reinforced Composite Materials for Craniofacial Bone Reconstruction. *The Journal of Craniofacial Surgery*, *27*(7), 1694–1699. https://doi.org/10.1097/SCS.0000000000002925

Le Bell-Rönnlöf, A.-M., Lassila, L. V. J., Kangasniemi, I., & Vallittu, P. K. (2011). Load-bearing capacity of human incisor restored with various fiber-reinforced composite posts. *Dental Materials: Official Publication of the Academy of Dental Materials*, *27*(6), e107-115. https://doi.org/10.1016/j.dental.2011.02.009

Lee, C.-T., Huang, Y.-W., Zhu, L., & Weltman, R. (2017). Prevalences of peri-implantitis and peri-implant mucositis: Systematic review and meta-analysis. *Journal of Dentistry*, *62*, 1–12. https://doi.org/10.1016/j.jdent.2017.04.011

Lee, H. C., Song, B., Kim, J. S., Jung, J. J., Li, H. H., Mutic, S., & Park, J. C. (2017). Variable step size methods for solving simultaneous algebraic reconstruction technique (SART)-type CBCT reconstructions. *Oncotarget*, *8*(20), 33827–33835. https://doi.org/10.18632/oncotarget.17385

Little, R. E., Long, C. M., Loehrl, T. A., & Poetker, D. M. (2018). Odontogenic sinusitis: A review of the current literature: Odontogenic Sinusitis and Current Literature. *Laryngoscope Investigative Otolaryngology*, *3*(2), 110–114. https://doi.org/10.1002/lio2.147

Liugang, G., Jianfeng, S., Tao, L., Kai, X., & Xinye, N. (2020). Metal Artifact Reduction Method Based on Noncoplanar Scanning in CBCT Imaging. *IEEE Access*, *8*, 7236–7243. https://doi.org/10.1109/ACCESS.2019.2962386

Loose, M., Rosentritt, M., Leibrock, A., Behr, M., & Handel, G. (1998). In vitro study of fracture strength and marginal adaptation of fibre-reinforced-composite versus all ceramic fixed partial dentures. *The European Journal of Prosthodontics and Restorative Dentistry*, *6*(2), 55–62.

Luckow, M., Deyhle, H., Beckmann, F., Dagassan-Berndt, D., & Müller, B. (2011). Tilting the jaw to improve the image quality or to reduce the dose in cone-beam computed tomography. *European Journal of Radiology*, *80*(3), e389–e393. https://doi.org/10.1016/j.ejrad.2010.10.001

Mahesh, K., Deshpande, P., & Viveka, S. (2022). Prevalence of artifacts in cone-beam computed tomography: A retrospective study. *Journal of Indian Academy of Oral Medicine and Radiology*, *34*(4), 428. https://doi.org/10.4103/jiaomr.jiaomr_142_22

Maillet, M., Bowles, W. R., McClanahan, S. L., John, M. T., & Ahmad, M. (2011). Cone-beam Computed Tomography Evaluation of Maxillary Sinusitis. *Journal of Endodontics*, *37*(6), 753–757. https://doi.org/10.1016/j.joen.2011.02.032

Mallya, S. M., Lam, E. W. N., White, S. C., & Pharoah, M. J. (2019). *White and Pharoah's oral radiology: Principles and interpretation* (8th edition). Elsevier.

Mancini, A. X. M., Santos, M. U. C., Gaêta-Araujo, H., Tirapelli, C., Pauwels, R., & Oliveira-Santos, C. (2021). Artefacts at different distances from titanium and zirconia implants in cone-beam computed tomography: Effect of tube current and metal artefact reduction. *Clinical Oral Investigations*, *25*(8), 5087–5094. https://doi.org/10.1007/s00784-021-03821-y

Matsumoto, Y., Ikeda, T., Yokoi, H., & Kohno, N. (2015). Association between odontogenic infections and unilateral sinus opacification. *Auris Nasus Larynx*, *42*(4), 288–293. https://doi.org/10.1016/j.anl.2014.12.006

Meirinhos, J., Martins, J. N. R., Pereira, B., Baruwa, A., Gouveia, J., Quaresma, S. A., Monroe, A., & Ginjeira, A. (2020). Prevalence of apical periodontitis and its association with previous root canal treatment, root canal filling length and type of coronal restoration – a cross-sectional study. *International Endodontic Journal*, *53*(4), 573–584. https://doi.org/10.1111/iej.13256

Meyer, E., Raupach, R., Lell, M., Schmidt, B., & Kachelrieß, M. (2010). Normalized metal artifact reduction (NMAR) in computed tomography: Normalized metal artifact reduction (NMAR) in computed tomography. *Medical Physics*, *37*(10), 5482–5493. https://doi.org/10.1118/1.3484090

Min, C.-K., & Kim, K.-A. (2021a). Quantitative analysis of metal artefacts of dental implant in CBCT image by correlation analysis to micro-CT: A microstructural study. *Dentomaxillofacial Radiology*, *50*(3), 20200365. https://doi.org/10.1259/dmfr.20200365

Min, C.-K., & Kim, K.-A. (2021b). Reducing metal artifacts between implants in cone-beam CT by adjusting angular position of the subject. *Oral Radiology*, *37*(3), 385–394. https://doi.org/10.1007/s11282-020-00458-7

Minnema, J., Eijnatten, M., Hendriksen, A. A., Liberton, N., Pelt, D. M., Batenburg, K. J., Forouzanfar, T., & Wolff, J. (2019). Segmentation of dental cone-beam CT scans affected by metal artifacts using a mixed-scale dense convolutional neural network. *Medical Physics*, *46*(11), 5027–5035. https://doi.org/10.1002/mp.13793

Moshfeghi, M., Safi, Y., Różyło-Kalinowska, I., & Gandomi, S. (2022). Does the size of an object containing dental implant affect the expression of artifacts in cone beam computed tomography imaging? *Head & Face Medicine*, *18*(1), 20. https://doi.org/10.1186/s13005-022-00326-1

Nagendrababu, V., Segura-Egea, J. J., Fouad, A. F., Pulikkotil, S. J., & Dummer, P. M. H. (2020). Association between diabetes and the outcome of root canal treatment in adults: An umbrella review. *International Endodontic Journal*, *53*(4), 455–466. https://doi.org/10.1111/iej.13253

Nair, P. N. R. (1997). Apical periodontitis: A dynamic encounter between root canal infection and host response. *Periodontology 2000*, *13*(1), 121–148. https://doi.org/10.1111/j.1600-0757.1997.tb00098.x

Nair, P. N. R. (2004). P ATHOGENESIS OF A PICAL P ERIODONTITIS AND THE C AUSES OF E NDODONTIC F AILURES. *Critical Reviews in Oral Biology & Medicine*, *15*(6), 348–381. https://doi.org/10.1177/154411130401500604

Najeeb, S., Mali, M., Syed, A. U. Y., Zafar, M. S., Khurshid, Z., Alwadaani, A., & Matinlinna, J. P. (2019). Dental implants materials and surface treatments. In *Advanced Dental Biomaterials* (pp. 581–598). Elsevier. https://doi.org/10.1016/B978-0-08-102476-8.00021-9

Nardi, C., Borri, C., Regini, F., Calistri, L., Castellani, A., Lorini, C., & Colagrande, S. (2015). Metal and motion artifacts by cone beam computed tomography (CBCT) in dental and maxillofacial study. *La Radiologia Medica*, *120*(7), 618–626. https://doi.org/10.1007/s11547-015-0496-2

Nomier, A. S., Gaweesh, Y. S. E.-D., Taalab, M. R., & El Sadat, S. A. (2022). Efficacy of low-dose cone beam computed tomography and metal artifact reduction tool for assessment of peri-implant bone defects: An in vitro study. *BMC Oral Health*, *22*(1), 615. https://doi.org/10.1186/s12903-022-02663-8

Oenning, A. C., Jacobs, R., Pauwels, R., Stratis, A., Hedesiu, M., & Salmon, B. (2018). Cone-beam CT in paediatric dentistry: DIMITRA project position statement. *Pediatric Radiology*, *48*(3), 308–316. https://doi.org/10.1007/s00247-017-4012-9

Ozcan, M., van der Sleen, J. M., Kurunmäki, H., & Vallittu, P. K. (2006). Comparison of repair methods for ceramic-fused-to-metal crowns. *Journal of Prosthodontics: Official Journal of the American College of Prosthodontists*, *15*(5), 283–288. https://doi.org/10.1111/j.1532-849X.2006.00124.x

Özkurt, Z., & Kazazoğlu, E. (2011). Zirconia Dental Implants: A Literature Review. *Journal of Oral Implantology*, *37*(3), 367–376. https://doi.org/10.1563/AAID-JOI-D-09-00079

Pauwels, R., Araki, K., Siewerdsen, J. H., & Thongvigitmanee, S. S. (2015). Technical aspects of dental CBCT: State of the art. *Dentomaxillofacial Radiology*, *44*(1), 20140224. https://doi.org/10.1259/dmfr.20140224

Pauwels, R., Jacobs, R., Singer, S. R., & Mupparapu, M. (2015). CBCT-based bone quality assessment: Are Hounsfield units applicable? *Dentomaxillofacial Radiology*, *44*(1), 20140238. https://doi.org/10.1259/dmfr.20140238

Pauwels, R., Stamatakis, H., Bosmans, H., Bogaerts, R., Jacobs, R., Horner, K., Tsiklakis, K., & The SEDENTEXCT Project Consortium. (2013). Quantification of metal artifacts on cone beam computed tomography images. *Clinical Oral Implants Research*, *24*, 94–99. https://doi.org/10.1111/j.1600-0501.2011.02382.x

Peltola, J., Ekholm, M., Huumonen, S., Peltonen, E., & Tammisalo, T. (2011). *STUK opastaa, KKTT-laitteen käyttö*. STUK.

Peltola, M. J., Vallittu, P. K., Vuorinen, V., Aho, A. A. J., Puntala, A., & Aitasalo, K. M. J. (2012). Novel composite implant in craniofacial bone reconstruction. *European Archives of Oto-Rhino-Laryngology*, *269*(2), 623–628. https://doi.org/10.1007/s00405-011-1607-x

Piitulainen, J. M., Mattila, R., Moritz, N., & Vallittu, P. K. (2017). Load-Bearing Capacity and Fracture Behavior of Glass Fiber-Reinforced Composite Cranioplasty Implants. *Journal of Applied Biomaterials & Functional Materials*, *15*(4), e356–e361. https://doi.org/10.5301/jabfm.5000375

Piitulainen, J. M., Posti, J. P., Aitasalo, K. M. J., Vuorinen, V., Vallittu, P. K., & Serlo, W. (2015). Paediatric cranial defect reconstruction using bioactive fibre-reinforced composite implant: Early outcomes. *Acta Neurochirurgica*, *157*(4), 681–687. https://doi.org/10.1007/s00701-015-2363-2

Posti, J. P., Piitulainen, J. M., Hupa, L., Fagerlund, S., Frantzén, J., Aitasalo, K. M. J., Vuorinen, V., Serlo, W., Syrjänen, S., & Vallittu, P. K. (2016). A glass fiber-reinforced composite – bioactive glass cranioplasty implant: A case study of an early development stage implant removed due to a late infection. *Journal of the Mechanical Behavior of Biomedical Materials*, *55*, 191–200. https://doi.org/10.1016/j.jmbbm.2015.10.030

Puglisi, S., Privitera, S., Maiolino, L., Serra, A., Garotta, M., Blandino, G., & Speciale, A. (2011). Bacteriological findings and antimicrobial resistance in odontogenic and non-odontogenic chronic maxillary sinusitis. *Journal of Medical Microbiology*, *60*(9), 1353–1359. https://doi.org/10.1099/jmm.0.031476-0

Radiation Protection 172. (2012). *Cone Beam CT for dental and maxillofacial radiology—Evidence-based Guidelines*. Publ Eur Communities.

Rajendran, K., Walsh, M. F., de Ruiter, N. J. A., Chernoglazov, A. I., Panta, R. K., Butler, A. P. H., Butler, P. H., Bell, S. T., Anderson, N. G., Woodfield, T. B. F., Tredinnick, S. J., Healy, J. L., Bateman, C. J., Aamir, R., Doesburg, R. M. N., Renaud, P. F., Gieseg, S. P., Smithies, D. J., Mohr, J. L., … Billinghurst, M. (2014). Reducing beam hardening effects and metal artefacts in spectral CT using Medipix3RX. *Journal of Instrumentation*, *9*(03), P03015–P03015. https://doi.org/10.1088/1748-0221/9/03/P03015

Rantala, L. I., Lastumäki, T. M., Peltomäki, T., & Vallittu, P. K. (2003). Fatigue resistance of removable orthodontic appliance reinforced with glass fibre weave: FATIGUE OF REINFORCED APPLIANCE. *Journal of Oral Rehabilitation*, *30*(5), 501–506. https://doi.org/10.1046/j.1365-2842.2003.01108.x

Rees, T. D., Biggs, N. L., & Collings, C. K. (1971). Radiographic interpretation of periodontal osseous lesions. *Oral Surgery, Oral Medicine, Oral Pathology*, *32*(1), 141–153. https://doi.org/10.1016/0030-4220(71)90260-X

Rehani, M. M., Gupta, R., Bartling, S., Sharp, G. C., Pauwels, R., Berris, T., & Boone, J. M. (2015). ICRP Publication 129: Radiological Protection in Cone Beam Computed Tomography (CBCT). *Annals of the ICRP*, *44*(1), 7–127. https://doi.org/10.1177/0146645315575485

Reti, R., & Findlay, D. (Eds.). (2021). *Oral board review for oral and maxillofacial surgery*. Springer.

Saibene, A. M., Vassena, C., Pipolo, C., Trimboli, M., De Vecchi, E., Felisati, G., & Drago, L. (2016). Odontogenic and rhinogenic chronic sinusitis: A modern microbiological comparison: Odonto- and rhinogenic sinusitis microbiology. *International Forum of Allergy & Rhinology*, *6*(1), 41–45. https://doi.org/10.1002/alr.21629

Saini, M. (2015). Implant biomaterials: A comprehensive review. *World Journal of Clinical Cases*, *3*(1), 52. https://doi.org/10.12998/wjcc.v3.i1.52

Salemi, F. (2021). Efficacy of Metal Artifact Reduction Algorithm of Cone-Beam Computed Tomography for Detection of Fenestration and Dehiscence around Dental Implants. *Journal of Biomedical Physics and Engineering*, *11*(3). https://doi.org/10.31661/jbpe.v0i0.2102-1284

Salvi, G. E., & Ramseier, C. A. (2015). Efficacy of patient-administered mechanical and/or chemical plaque control protocols in the management of peri-implant mucositis. A systematic review. *Journal of Clinical Periodontology*, *42 Suppl 16*, S187-201. https://doi.org/10.1111/jcpe.12321

Sasaki, H., Hirai, K., M. Martins, C., Furusho, H., Battaglino, R., & Hashimoto, K. (2016). Interrelationship Between Periapical Lesion and Systemic Metabolic Disorders. *Current Pharmaceutical Design*, *22*(15), 2204–2215. https://doi.org/10.2174/1381612822666160216145107

Scarfe, W. C., & Angelopoulos, C. (Eds.). (2018). *Maxillofacial cone beam computed tomography: Principles, techniques and clinical applications*. Springer. https://doi.org/10.1007/978-3-319-62061-9

Scarfe, W. C., & Farman, A. G. (2008). What is Cone-Beam CT and How Does it Work? *Dental Clinics of North America*, *52*(4), 707–730. https://doi.org/10.1016/j.cden.2008.05.005

Schriber, M., Yeung, A. W. K., Suter, V. G. A., Buser, D., Leung, Y. Y., & Bornstein, M. M. (2020). Cone beam computed tomography artefacts around dental implants with different materials influencing the detection of peri-implant bone defects. *Clinical Oral Implants Research*, *31*(7), 595–606. https://doi.org/10.1111/clr.13596

Schulze, R. (2013). *The National German Guidelines*.

Schulze, R. (2022). CBCT artefact-burden of zirconia-based as compared to titanium implants for different beam energies: An analytical approach. *Scientific Reports*, *12*(1), 15276. https://doi.org/10.1038/s41598-022-19379-y

Schulze, R., Heil, U., Groβ, D., Bruellmann, D., Dranischnikow, E., Schwanecke, U., & Schoemer, E. (2011). Artefacts in CBCT: A review. *Dentomaxillofacial Radiology*, *40*(5), 265–273. https://doi.org/10.1259/dmfr/30642039

Schulze, R. K. W., Berndt, D., & D'Hoedt, B. (2010). On cone-beam computed tomography artifacts induced by titanium implants: Titanium artifacts in CBCT. *Clinical Oral Implants Research*, *21*(1), 100–107. https://doi.org/10.1111/j.1600-0501.2009.01817.x

Schwarz, F., Becker, K., & Sager, M. (2015). Efficacy of professionally administered plaque removal with or without adjunctive measures for the treatment of peri-implant mucositis. A systematic review and meta-analysis. *Journal of Clinical Periodontology*, *42 Suppl 16*, S202-213. https://doi.org/10.1111/jcpe.12349

Sewón, L. A., Ampula, L., & Vallittu, P. K. (2000). Rehabilitation of a periodontal patient with rapidly progressing marginal alveolar bone loss: 1-year follow-up. *Journal of Clinical Periodontology*, *27*(8), 615–619. https://doi.org/10.1034/j.1600-051x.2000.027008615.x

Shanbhag, S., Karnik, P., Shirke, P., & Shanbhag, V. (2013). Association between Periapical Lesions and Maxillary Sinus Mucosal Thickening: A Retrospective Cone-beam Computed Tomographic Study. *Journal of Endodontics*, *39*(7), 853–857. https://doi.org/10.1016/j.joen.2013.04.010

Sheikhi, M., Behfarnia, P., Mostajabi, M., & Nasri, N. (2020). The efficacy of metal artifact reduction (MAR) algorithm in cone-beam computed tomography on the diagnostic accuracy of fenestration and dehiscence around dental implants. *Journal of Periodontology*, *91*(2), 209–214. https://doi.org/10.1002/JPER.18-0433

Siiskonen, T., Gallagher, A., Ciraj Bjelac, O., Novak, L., Sans Merce, M., Farah, J., Dabin, J., Malchair, F., Knežević, Ž., & Kortesniemi, M. (2021). A European perspective on dental cone beam computed tomography systems with a focus on optimisation utilising diagnostic reference levels. *Journal of Radiological Protection*, *41*(2), 442–451. https://doi.org/10.1088/1361-6498/abdd05

Sun, T., Jacobs, R., Pauwels, R., Tijskens, E., Fulton, R., & Nuyts, J. (2021). A motion correction approach for oral and maxillofacial cone-beam CT imaging. *Physics in Medicine & Biology*, *66*(12), 125008. https://doi.org/10.1088/1361-6560/abfa38

Sykaras, N., Iacopino, A. M., Marker, V. A., Triplett, R. G., & Woody, R. D. (2000). Implant materials, designs, and surface topographies: Their effect on osseointegration. A literature review. *The International Journal of Oral & Maxillofacial Implants*, *15*(5), 675–690.

The 2007 Recommendations of the International Commission on Radiological Protection. ICRP publication 103. (2007). *Annals of the ICRP*, *37*(2–4), 9–34. https://doi.org/10.1016/j.icrp.2007.10.003

Tibúrcio-Machado, C. S., Michelon, C., Zanatta, F. B., Gomes, M. S., Marin, J. A., & Bier, C. A. (2021). The global prevalence of apical periodontitis: A systematic review and meta-analysis. *International Endodontic Journal*, *54*(5), 712–735. https://doi.org/10.1111/iej.13467

Tschernitschek, H., Borchers, L., & Geurtsen, W. (2005). Nonalloyed titanium as a bioinert metal—A review. *Quintessence International (Berlin, Germany: 1985)*, *36*(7–8), 523–530.

Tuusa, S. M.-R., Peltola, M. J., Tirri, T., Puska, M. A., Röyttä, M., Aho, H., Sandholm, J., Lassila, L. V. J., & Vallittu, P. K. (2008). Reconstruction of critical size calvarial bone defects in rabbits with glass–fiber-reinforced composite with bioactive glass granule coating. *Journal of Biomedical Materials Research Part B: Applied Biomaterials*, *84B*(2), 510–519. https://doi.org/10.1002/jbm.b.30898

Vallittu, P. K. (1998). The effect of glass fiber reinforcement on the fracture resistance of a provisional fixed partial denture. *The Journal of Prosthetic Dentistry*, *79*(2), 125–130. https://doi.org/10.1016/s0022-3913(98)70204-5

Vallittu, P. K. (2016). Are we misusing fiber posts? Guest editorial. *Dental Materials: Official Publication of the Academy of Dental Materials*, *32*(2), 125–126. https://doi.org/10.1016/j.dental.2015.11.001

Vallittu, P. K. (2017). Bioactive glass-containing cranial implants: An overview. *Journal of Materials Science*, *52*(15), 8772–8784. https://doi.org/10.1007/s10853-017-0888-x

Vallittu, P. K. (2018). An overview of development and status of fiber-reinforced composites as dental and medical biomaterials. *Acta Biomaterialia Odontologica Scandinavica*, *4*(1), 44–55. https://doi.org/10.1080/23337931.2018.1457445

Vallittu, P., & Özcan, M. (Eds.). (2017). *Clinical guide to principles of fiber-reinforced composites in dentistry*. Elsevier, Woodhead Publishing.

Varley, D., Yousaf, S., Youseffi, M., Mozafari, M., Khurshid, Z., & Sefat, F. (2019). Fiber-reinforced composites. In *Advanced Dental Biomaterials* (pp. 301–315). Elsevier. https://doi.org/10.1016/B978-0-08-102476-8.00013-X

Vasconcelos, K. de F., Codari, M., Queiroz, P. M., Nicolielo, L. F. P., Freitas, D. Q., Sforza, C., Jacobs, R., & Haiter-Neto, F. (2019). The performance of metal artifact reduction algorithms in cone beam computed tomography images considering the effects of materials, metal positions, and fields of view. *Oral Surgery, Oral Medicine, Oral Pathology and Oral Radiology*, *127*(1), 71–76. https://doi.org/10.1016/j.oooo.2018.09.004

Vidal, F., Coutinho, T. M., Carvalho Ferreira, D. D., Souza, R. C. D., & Gonçalves, L. S. (2017). Odontogenic sinusitis: A comprehensive review. *Acta Odontologica Scandinavica*, *75*(8), 623–633. https://doi.org/10.1080/00016357.2017.1372803

Wang, T., Matinlinna, J. P., Burrow, M. F., & Ahmed, K. E. (2021). The biocompatibility of glass-fibre reinforced composites (GFRCs) – a systematic review. *Journal of Prosthodontic Research*, *65*(3), 273–283. https://doi.org/10.2186/jpr.JPR_D20_00031

Warren, E. K., Vaddi, A., & Tadinada, A. (2022). A comparative evaluation of the metallic artifact generated by a ceramic dental implant and a titanium dental implant imaged on cone-beam computed tomographic scans. *JADA Foundational Science*, *1*, 100007. https://doi.org/10.1016/j.jfscie.2022.100007

Whaites, E., & Drage, N. (2015). *Essentials of dental radiography and radiology* (5th ed., reprint). Churchill Livingstone Elsevier.

Zhang, Y., Zhang, L., Zhu, X. R., Lee, A. K., Chambers, M., & Dong, L. (2007). Reducing metal artifacts in cone-beam CT images by preprocessing projection data. *International Journal of Radiation Oncology*Biology*Physics*, *67*(3), 924–932. https://doi.org/10.1016/j.ijrobp.2006.09.045

Zirk, M., Dreiseidler, T., Pohl, M., Rothamel, D., Buller, J., Peters, F., Zöller, J. E., & Kreppel, M. (2017). Odontogenic sinusitis maxillaris: A retrospective study of 121 cases with surgical intervention. *Journal of Cranio-Maxillofacial Surgery*, *45*(4), 520–525. https://doi.org/10.1016/j.jcms.2017.01.023

TURUN
YLIOPISTO
UNIVERSITY
OF TURKU

Painosalama, Turku, Finland 2023

ISBN 978-951-29-9500-4 (Print)
ISBN 978-951-29-9501-1 (PDF)
ISSN 0355-9483 (Print)
ISSN 2343-3213 (Online)